16. Shimono, K., Shimono, Y., Shimokata, K., Ishiguro, N., and Takahashi, M.
Microspherule protein 1, Mi-2β, and RET finger protein associate in the nucleolus and up-regulate ribosomal gene transcription.
J. Biol. Chem. 280: 39436-39447 (2005).

17. Murakumo, Y., Mizutani, S., Yamaguchi, M., Ichihara, M. and Takahashi, M.
Analyses of ultraviolet-induced focus formation of hREV1 protein.
Genes Cells 11: 193-205 (2006).

18. Takeda, K., Kawamoto, Y., Okuno, Y, Kato, M., Takahashi, M., Suzuki, H., Isobe, K. and Nakashima, I.
A PKC-mediated backup mechanism of the MXXCW motif-linked switch for initiating tyrosine kinase activities.
FEBS Lett. 580:839-843 (2006).

19. Asai, N., Jijiwa, M., Enomoto, A., Kawai, K., Maeda, K., Ichihara, M. and Takahashi M.
RET receptor signaling; Dysfunction in thyroid cancer and Hirschsprung's disease.
Pathol Int. 56: 164-172 (2006).

20. Kato, M., Takeda, K., Kawamoto, Y., Tsuzuki, T., Kato, Y., Ohno, T., Hossain, K., Iftakhar-E-Khuda, I., Ohgami, N., Isobe, K., Takahashi, M.and Nakashima, I.
Novelhairless RET-transgenic mouse line with melanocytic nevi and anagen hairfollicles.
J. Invest. Dermatol. 126: 2547-2550 (2006).

21. Uchida, M., Enomoto, A., Fukuda, T., Kurokawa, K., Maeda, K., Kodama, Y., Asai, N., Hasegawa, T., Shimono, Y., Jijiwa, M., Ichihara, M., Murakumo, Y. and Takahashi, M.
Dok-4 regulates GDNF-dependent neurite outgrowth through downstream activation of Rap1 and mitogen-activated protein kinase.
J. Cell Sci. 119: 3067-3077 (2006).

22. Asai, N., Fukuda, T., Wu, Z., Enomoto, A., Pachnis, V., Takahashi, M. and Costantini, F.
Targeted mutation of serine 697 in the Ret tyrosine kinase causes migration defect of enteric neural crest cells.
Development 133: 4507-4516 (2006).

23. Murakumo, M., Jijiwa, M., Asai, N., Ichihara, M., and Takahashi, M.
RET and neuroendocrine tumors.
Pituitary 9: 179-192 (2006).

24. Enomoto, A., Jiang, P., and Takahashi, M.
Girdin, a novel actin-binding protein, and

its family of proteins posses versatile function in the Akt and Wnt signaling pathways.
Ann. NY Acad. Sci., 1086: 169-184 (2006).

25. Kato, M., Ohgami, N., Kawamoto, Y., Tsuzuki, T., Hossain, K., Yanagishita, T., Ohshima, Y., Tsuboi, H., Yamanoshita, O., Matsumoto, Y., Takahashi, M. and Nakashima, I.
Protective effect of hyperpigmented skin on UV-mediated cutaneous cancer development.
J. Invest. Dermatol. in press.

G. 学会発表

(ア) 浅井直也、高橋雅英
PKAによるRetリン酸化部位の変異で生じるHirschsprung病類似の病態の解析
第94回日本病理学会総会　2005年4月

(イ) 時々輪真由美、川井久美、村雲芳樹、高橋雅英
RET チロシン 1062 を介するシグナルの欠如は精子形成に異常をきたす
第94回日本病理学会総会　2005年4月

(ウ) 内田真由美、黒川　景、高橋雅英
RET受容体型チロシンキナーゼの細胞内シグナル伝達系におけるアダプタータンパク質Dok-4の役割
第64回日本癌学会学術総会　2005年9月

(エ) 内田真由美、榎本　篤、高橋雅英
神経分化における RET チロシンキナーゼとアダプタータンパク質Dok-4の機能解析
第95回日本病理学会学術総会　2006年5月

(オ) 浅井直也、高橋雅英
神経堤細胞の移動による腸管神経形成に作用するシグナルの解析
第95回日本病理学会学術総会　2006年5月

(カ) 石田麻紀、市原正智、村雲芳樹、高橋雅英
RET受容体型チロシンキナーゼのシグナル伝達系におけるSprouty蛋白質の機能解析
第 65 回日本癌学会学術総会　2006 年 9 月

(キ) 石田麻紀、市原正智、村雲芳樹、高橋雅英
RET受容体型チロシンキナーゼのシグナル伝達系におけるSprouty蛋白質の機能解析
日本分子生物学会フォーラム 2006
2006年12月

(ク) 浅井直也、福田敏史、榎本　篤、高橋雅英
Retチロシンキナーゼの S697A 変異によって胎生期の腸管神経前駆細胞の移動が障害される
日本分子生物学会フォーラム 2006
2006年12月

III. 研究成果の刊行に関する一覧表

Ito S, Sawada M, Haneda M, Fujii S, Oh-Hashi K, Kiuchi K, Takahashi M, Isobe K. Amyloid-beta peptides induce cell proliferation and macrophage colony-stimulating factor expression via the PI3-kinase/Akt pathway in cultured Ra2 microglial cells.
FEBS Lett. 2005 Mar 28;579(9):1995-2000.

Ito S, Sawada M ,Haneda M, Ishida Y, Isobe KI. Amyloid-beta peptides induce several chemokine mRNA expressions in the primary microglia and Ra2 cell line via the PI3K/Akt and/or ERK pathway. Neurosci Res. 2006 2006 Nov;56(3):294-9.

Waza M,Adachi H, Katsuno M, Minamiyama M, Sang C, Nakagomi Y, Kobayashi Y, Tanaka F, Doyu M, Inukai A, Yoshida M, Hashizume Y and Sobue G. 17-AAG, an Hsp90 inhibitor,ameliorates polyglutamine-mediated motor neuron degeneration. Nat Med 11: 1088-1095, 2005.

Enomoto A, Murakami H, Asai N, Morone N, Watanabe T, Kawai K, Murakumo Y, Usukura J, Kaibuchi K, Takahashi M. Akt/PKB regulates actin organization and cell motility via Girdin/APE. Dev Cell. 2005 Sep;9(3):389-402.

Hayashi T, Juliet PA, Matsui-Hirai H, Miyazaki A, Fukatsu A, Funami J, Iguchi A, Ignarro LJ. l-Citrulline and l-arginine supplementation retards the progression of high-cholesterol-diet-induced atherosclerosis in rabbits. Proc Natl Acad Sci U S A. 2005;102:13681-6.

Amyloid-β peptides induce cell proliferation and macrophage colony-stimulating factor expression via the PI3-kinase/Akt pathway in cultured Ra2 microglial cells

Sachiko Ito[a], Makoto Sawada[b], Masataka Haneda[a,1], Satoshi Fujii[c], Kentaro Oh-hashi[c], Kazutoshi Kiuchi[c], Masahide Takahashi[d], Ken-ichi Isobe[a,*,1]

[a] *Department of Basic Gerontology, National Institute for Longevity Sciences, 36-3 Gengo, Morioka-cho, Obu, Aichi 474-8522, Japan*
[b] *Institute for Comprehensive Medical Science, Fujita Health University, Toyoake, Aichi 470-1192, Japan*
[c] *Department of Biomolecular Science, Faculty of Engineering, Gifu University, Yanagido, Gifu 501-1193, Japan*
[d] *Department of Pathology, Nagoya University Graduate School of Medicine, 65 Tsurumai-cho, Showa-ku, Nagoya 466-8550, Japan*

Received 28 December 2004; revised 8 February 2005; accepted 21 February 2005

Available online 5 March 2005

Edited by Jesus Avila

Abstract Alzheimer's disease is characterized by numerous amyloid-β peptide (Aβ) plaques surrounded by microglia. Here we report that Aβ induces the proliferation of the mouse microglial cell line Ra2 by increasing the expression of macrophage colony-stimulating factor (M-CSF). We examined signal cascades for Aβ-induced M-CSF mRNA expression. The induction of M-CSF was blocked by a phosphatidylinositol 3 kinase (PI3-kinase) inhibitor (LY294002), a Src family tyrosine kinase inhibitor (PP1) and an Akt inhibitor. Electrophoretic mobility shift assays showed that Aβ enhanced NF-κB binding activity to the NF-κB site of the mouse M-CSF promoter, which was blocked by LY294002. These results indicate that Aβ induces M-CSF mRNA expression via the PI3-kinase/Akt/NF-κB pathway.

Keywords: Microglia; Alzheimer's disease; Amyloid-β; Akt; NF-κB; Macrophage colony-stimulating factor

1. Introduction

Alzheimer's disease (AD) is characterized by the presence of senile plaques in the brain composed primarily of amyloid-β peptide (Aβ). Microglia have been reported to surround the Aβ plaques, which provokes a microglia-mediated inflammatory response that contributes to neuronal cell loss [1]. On the other hand, microglia play an important role in the clearance of Aβ by phagocytosis, primarily through scavenger receptor class A (SR-A, CD204), scavenger receptor-BI (SR-BI) and CD36 [2–4]. Recently, it has been reported that microglia isolated from CD36-deficient mice had marked reductions in Aβ-induced cytokine/chemokine secretion [5]. CD36 binds to Aβ in vitro [6], and is physically associated with members of the Src family tyrosine kinase [7,8], which transduce signals from this receptor [9]. Another receptors such as receptor for advanced glycosylation end-products (RAGE), integrins and heparan sulfate proteoglycans, also have been reported to bind with Aβ [10].

There are many reports that microglia are activated by Aβ, but it has been unclear whether Aβ is associated with the proliferation of microglia. Here we report that Aβ induces proliferation of the microglial cell line Ra2 by increasing macrophage colony-stimulating factor (M-CSF) expression. We also elucidated signal transduction pathways from Aβ-treatment to M-CSF mRNA expression in microglia.

2. Materials and methods

2.1. Materials

Synthetic human Aβ25–35, Aβ1–42 and Aβ1–16 were obtained from Peptide Institute Inc. Aβ35–25 was from AnaSpec Inc. Aβ25–35, Aβ1–16 and Aβ35–25 were dissolved in H_2O and Aβ 1–42 was dissolved in 0.1% NH_3 according to the manufacturer's instructions. Anti-phospho-Akt (Serine 473), anti-Akt, anti-phospho-IκBα (Serine 32), and anti-IκBα antibodies were from Cell Signaling. PP1 was from Biomol. Wortmannin, LY294002 and Akt inhibitor [1L-6-hydroxymethyl-chiro-inositol 2-(*R*)-2-*O*-methyl-3-*O*-octadecylcarbonate] were from Calbiochem. Piceatannol was from Sigma–Aldrich. Mouse recombinant granulocyte–macrophage colony-stimulating factor (mrGM-CSF) was from Pharmingen. Mouse recombinant M-CSF (mrM-CSF) was from Techne. Aβ25-35 and Aβ1–42 were used at 50 and 10 μM, respectively, in all studies unless otherwise stated.

2.2. Cell culture

Microglial cell line Ra2 was cultured in MGI medium [Eagle's MEM supplemented with 0.2% glucose, 5 μg/ml bovine Insulin (Sigma–Aldrich), and 10% fetal bovine serum (FBS, Invitrogen)] and 0.8 ng/ml mrGM-CSF (Pharmingen) [11]. Before Aβ-treatment, Ra2 cells were cultured in MGI medium without mrGM-CSF for 16 h. Primary microglia and primary astrocytes were prepared using newborn C57BL/6 mice as described previously [12], and cultured in MGI medium containing 0.8 ng/ml mrGM-CSF. The neuroblastoma cell line Neuro2a was cultured in DMEM supplemented with 10% FBS. Primary neurons were obtained from the cortex of 14-day-old C57BL/6 mouse embryos as described previously [13] with some modifications. Neural cells cultured in DMEM supplemented with TIS (5 μg/ml

*Corresponding author. Fax: +81 52 744 2972.
E-mail address: kisobe@med.nagoya-u.ac.jp (K. Isobe).

[1] Present address. Department of Immunology, Nagoya University Graduate School of Medicine, 65 Tsurumai-cho, Showa-ku, Nagoya 466-8550, Japan.

Abbreviations: AD, Alzheimer's disease; Aβ, amyloid-β; EMSA, electrophoretic mobility shift assay; FBS, fetal bovine serum; GM-CSF, granulocyte–macrophage colony stimulating factor; M-CSF, macrophage colony-stimulating factor; PBS, phosphate-buffered saline; PI3-kinase, phosphatidylinositol 3 kinase; RAGE, receptor for advanced glycation end-products

0014-5793/$30.00
doi:10.1016/j.febslet.2005.02.048

transferrin, 5 μg/ml insulin, and 5 ng/ml selenite, Sigma), 10% FBS and 5 μM cytosine arabinoside (Ara-C, Sigma). Before Aβ-treatment, primary neurons were cultured in MGI medium for 16 h.

2.3. Cell proliferation (WST-1) assay

Cell proliferation was determined by analyzing the conversion of WST-1 (light red) to its formazan derivate (dark red) using a WST-1 Cell Counting Kit (Dotite). For neutralization of M-CSF, anti-mouse M-CSF antibody (Techne) was added to the culture medium. At the end of the experiments, the media were replaced, and cells were incubated with 10 μl of the WST-1 reagent for 1 h at 37 °C in 5% CO_2. The absorbance at 450 nm was measured by using a microplate reader (Bio-Rad).

2.4. Immunoblotting

Cells were lysed in sample buffer (62.5 mM Tris–HCl, pH 6.8, 2% SDS, 10% glycerol, 5% 2-mercaptoethanol, and 5% bromophenol blue). Then 50 μg of total protein was resolved by SDS–PAGE and transferred to PVDF membranes (Millipore). Immunoblotting was performed with the appropriate antibody using the enhanced chemiluminescence (ECL) system (Amersham Pharmacia).

2.5. RT-PCR and real-time quantitative RT-PCR

Total RNA was isolated using an RNeasy mini kit (Qiagen) according to the manufacturer's instructions. Two micrograms of total RNA was reverse transcribed to cDNA using SuperScript II Reverse Transcriptase (Invitrogen). For RT-PCR and real-time quantitative PCR, the primers for mouse M-CSF and β-actin genes were as follows (5′ to 3′): M-CSF sense, CCATCGAGACCCTCAGACAT; M-CSF antisense1 for RT-PCR, CCTAAGGGAAAGGGTCCTGA; M-CSF antisense2 for real-time PCR, GATGAGGACAGACAGGTGGA; β-actin sense, AGTGTGACGTTGACATCCGT; and β-actin antisense, GCAGCTCAGTAACAGTCCGC. Conventional RT-PCR was performed using 0.5 μl cDNA, and 30 cycles of amplification for M-CSF or 23 cycles for β-actin at 94 °C for 1 min, 60 °C for 1 min and 72 °C for 1 min. Quantitative real-time PCR was performed on the Smart Cycler system (Takara) using the following program: 2 min at 50 °C, 10 min at 95 °C, followed by 40 cycles of 15 s at 95 °C, 1 min at 60 °C, and 8 s at 72 °C. The reactions were carried out using 0.5 μl cDNA with Smart Kit for Sybr Green I (Eurogentec). To check the specificity of reactions, a single band of the correct size was visualized by running out on 2% agarose gels. Values were expressed as relative expression of M-CSF mRNA normalized to the β-actin mRNA.

2.6. Nuclear extracts and electrophoretic mobility shift assays (EMSAs)

Nuclear extracts of Ra2 cells were prepared as previously described [14]. Three micrograms of nuclear extract was incubated with 5 fmol of ^{32}P end-labeled double-stranded oligonucleotides derived from M-CSF promoter in binding buffer [10 mM Tris, pH 7.5, 4% glycerol, 1 mM $MgCl_2$, 50 mM NaCl, 0.5 mM EDTA, 0.5 mM DTT, and 0.05 μg/μl poly(dI–dC)] for 20 min at room temperature. For competition assays, 1 pmol of unlabeled probe was incubated in the reaction mix before the addition of the ^{32}P-labeled probe. The oligonucleotides used in these experiments were as follows: NF-κB probe, 5′-GCCTTGAGGGAAAGTCCCTAGGGGC-3′; AP1 probe, 5′-GTAGTATGTGTCAGTGCC-3′. For supershift assays, nuclear extracts were preincubated with anti-NF-κB p50 or p65 antibodies (Santa Cruz) for 1 h at 4 °C. The DNA–protein complex was separated on 5% native polyacrylamide gels. The dried gels were visualized using an Image Reader (Fujifilm).

2.7. Statistical analysis

Results are expressed as means ± S.D. Statistical analysis was done by a two-tailed Student's *t* test. A P value of <0.05 was considered statistically significant.

3. Results and discussion

3.1. Aβ promotes microglial cell proliferation

To investigate the possible role of Aβ in the activation of microglia, we examined if Aβ could sustain the cell proliferation of microglial cell line Ra2. Ra2 cells proliferate in MGI medium containing GM-CSF and stop proliferating without GM-CSF [11]. Under MGI medium without GM-CSF, the effects of M-CSF or Aβ on the proliferation of Ra2 cells were analyzed by the WST-1 assay. The addition of M-CSF induced cell proliferation dose-dependently (Fig. 1A). Aβ25–35 increased Ra2 cell proliferation dose-dependently (Fig. 1B). Aβ25–35 does not occur naturally but has shown to mimic the effects of Aβ1–42 [15–17]. Aβ1–42, which occurs in a brain affected by AD, was more effective in cell proliferation than Aβ25–35 (Fig. 1C). It has been reported that Aβ stimulates the proliferation of microglia to enclose Aβ plaque [18,19]. We examined if M-CSF provoked the cell proliferation with Aβ-treatment. The effect of Aβ on the proliferation was blocked by anti-M-CSF antibody ($P < 0.05$) (Fig. 1D). The treatment with M-CSF was performed as a control. The effect of M-CSF was blocked by anti-M-CSF antibody (Fig. 1D). We found that Aβ induces microglial cell proliferation by M-CSF production.

3.2. Aβ induces M-CSF mRNA expression in microglia

To examine whether Aβ could induce M-CSF mRNA expression in microglia, Ra2 cells were stimulated with Aβ25–35 for 16 h at various concentrations. Aβ25–35 induced M-CSF mRNA expression dose-dependently (Fig. 2A). As a result of real-time quantitative RT-PCR (Fig. 2A, right), M-CSF mRNA induction by 50 μM Aβ25–35 was about sevenfold of non-treated control. Aβ25–35 induced time-dependent increases in M-CSF mRNA expression (Fig. 2B). Aβ1–42 also induced M-CSF expression (Fig. 2A and B). GM-CSF mRNA, on the other hand, was not induced by Aβ25–35 or Aβ1–42 (data not shown). Aβ1–16 did not induce M-CSF mRNA expression (Fig. 2C), nor

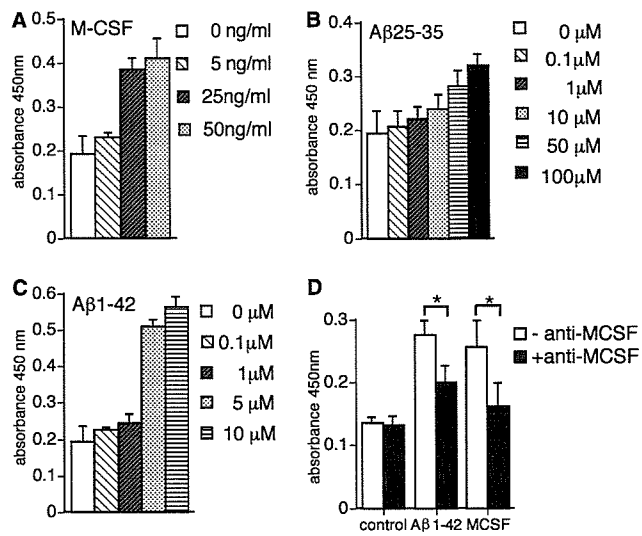

Fig. 1. Aβ promotes Ra2 cell proliferation. Cellular proliferation was measured by WST-1 assay. (A, B and C) Ra2 cells were incubated with the medium containing M-CSF, Aβ25–35 or Aβ1–42 at indicated concentrations for 48 h. (D) Ra2 cells were preincubated with 1 μg/ml anti-M-CSF antibody for 1 h before treatment with 5 μM Aβ1–42 or 25 ng/ml M-CSF for 24 h. Mean ± S.D. values from a single experiment were performed in triplicate. Similar results were obtained in each of two separate experiments (*$P < 0.05$).

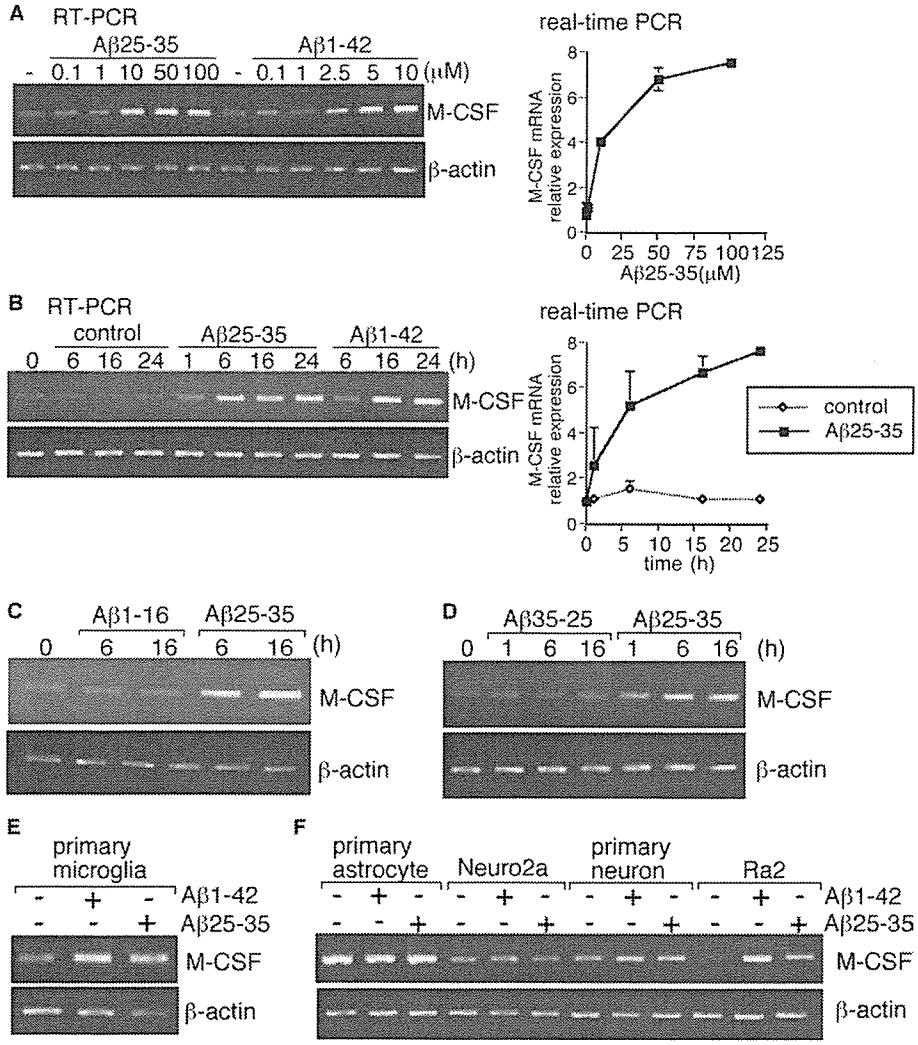

Fig. 2. Aβ stimulates M-CSF mRNA expression in microglia. (A and B) M-CSF and β-actin mRNA were determined by RT-PCR (left) and quantified by real-time PCR (right). Data represent means ± S.D. of three separate determinations. Ra2 cells were treated with Aβ25–35 or Aβ1–42 at indicated concentrations for 16 h (A). Time course of M-CSF relative expression of Ra2 cells treated with 50 μM Aβ25–35 and 10 μM Aβ1–42 (B). (C and D) Ra2 cells were treated with 50 μM Aβ1–16 (C) or 50 μM Aβ35–25 (D) for indicated times. (E and F) Primary microglia (E), primary neurons, primary astrocytes and neuroblastoma Neuro2a (F) were treated with 50 μM Aβ25–35 or 10 μM Aβ1–42 for 16 h.

did Aβ 35–25, which was a reverse sequence of Aβ25–35 (Fig. 2D). In primary microglia, as well as in Ra2 cells, Aβ25–35 and Aβ1–42 increased M-CSF mRNA expression (Fig. 2E). We also examined whether Aβ induced increases in M-CSF mRNA expression in primary astrocytes, primary neurons, and neuroblastoma cells Neuro2a. These cells constitutively expressed M-CSF mRNA, but Aβ25–35 and Aβ1–42 did not induce further expression of M-CSF mRNA (Fig. 2F). These results demonstrate that Aβ induced M-CSF mRNA expression in only microglia.

3.3. *Aβ induces M-CSF mRNA via Src family tyrosine kinase and PI3-kinase signal cascade*

Because our studies showed that Aβ25–35 had induced M-CSF expression in Ra2 cells, we examined signal cascades for Aβ-induced M-CSF mRNA expression by using several chemical inhibitors. The Src family tyrosine kinase is associated with CD36, which transduces signal cascades by Aβ [7,8,20]. In addition, Syk tyrosine kinase is activated by Aβ [21]. First, we examined if M-CSF mRNA expression was induced by Aβ via tyrosine kinase, Src family and Syk. A specific inhibitor of Src family kinase, PP1, prevented the increase in M-CSF mRNA induced by Aβ (Fig. 3A). A Syk-selective inhibitor, piceatannol, also blocked the increase in M-CSF mRNA expression (Fig. 3B). Next, to investigate whether the PI3-kinase pathway regulates Aβ-induced M-CSF expression, Ra2 cells were pretreated with the PI3-kinase inhibitors, wortmannin or LY294002. Wortmannin and LY294002 inhibited the increase in M-CSF mRNA expression dose-dependently (Fig. 3C and D). Fig. 3E shows the result of quantitative amounts of mRNA by real-time PCR. It has been reported that Aβ stimulates tyrosine kinase, PI3-kinase and Akt activation in neural and macrophage cells [21–24]. However, analysis of these signal transductions in microglia has not been reported. This is the first report that Aβ induces M-CSF expression through

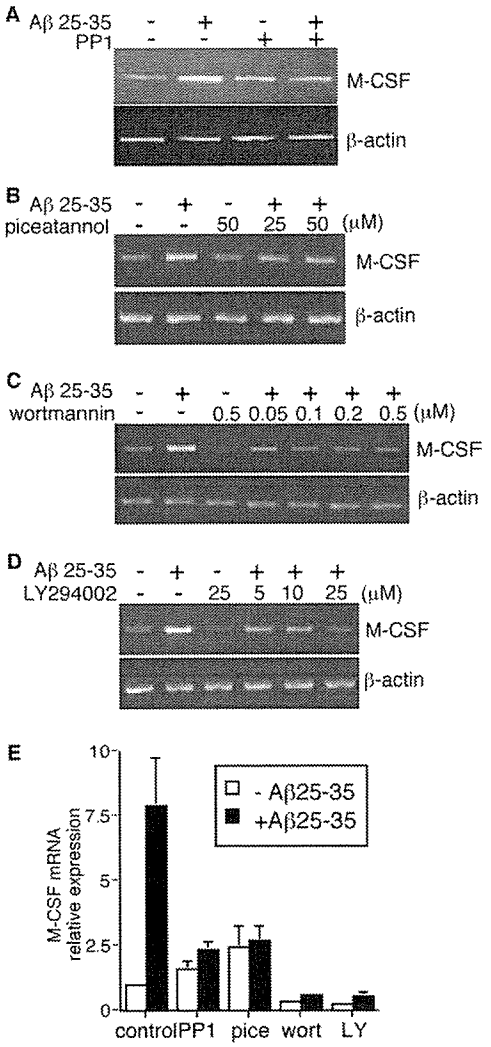

Fig. 3. Signal transduction for M-CSF mRNA expression induced by Aβ. (A–D) M-CSF and β-actin mRNA expression were determined by RT-PCR. Ra2 cells were preincubated with 10 μM PP1 (A), wortmannin (C), LY294002 (D) for 30 min or piceatannol (B) for 1 h before treatment of 50 μM Aβ25–35 for 6 h. Beacuse all inhibitors were dissolved in DMSO, control cells were treated with DMSO. (E) M-CSF mRNA expressions were measured by real-time PCR (pice, piceatannol; wort, wortmannin; LY, LY294002). Data represent means ± S.D. values of three separate determinations.

the Src family and Syk tyrosine kinases and the PI3-kinase in microglia.

3.4. Aβ activates Akt signaling pathway in microglia

We examined whether Akt was involved in the Aβ-induced M-CSF expression in Ra2 cells. Akt inhibitor blocked the increase of M-CSF mRNA expression (Fig. 4A). Immunoblotting analysis revealed that Akt was transiently phoshorylated at serine 473 by Aβ (Fig. 4B). LY294002 and PP1 suppressed the phosphorylation of Akt induced by Aβ (Fig. 4D). Piceatannol also blocked the phosphorylation of Akt (Fig. 4E). Because tyrosine kinases and PI3-kinase activate MEK/Erk/Elk [25,26], we examined whether these signal pathways were related to M-CSF mRNA expression induced by Aβ. Aβ induced MEK and Erk1/2 phosphorylation in Ra2 cells. However, specific inhibitors of MEK, U0126 and PD98059 did not inhibit Aβ-induced M-CSF mRNA expression (data not shown). These results indicate that the tyrosine kinases, Src family and Syk, and the PI3-kinase activate Akt for Aβ-induced M-CSF expression.

3.5. Aβ activates NF-κB via PI3-kinase signal cascade

Because NF-κB is a target of Akt [27], next we examined if IκBα phosphorylation was induced by Aβ. The phosphorylation of IκBα on serine 32 results in the release and nuclear translocation of active NF-κB [28]. IκBα was phosphorylated time-dependently, the phosphorylation peaked at 60 min and then declined (Fig. 4C). The phosphorylation was inhibited by LY294002 and PP1 (Fig. 4D). Piceatannol also blocked the phosphorylation of IκBα (Fig. 4E).

The M-CSF promoter region has a putative NF-κB binding site at −369–378 bp from the transcriptional start site [29]. To investigate whether this NF-κB binding site is associated with Aβ-induced M-CSF expression, EMSA was carried out with nuclear extracts prepared from untreated and Aβ-treated Ra2 cells. The amount of protein binding to the NF-κB probe was increased by Aβ-treatment (Fig. 5A, compare lanes 2 and 3). NF-κB binding activity was almost completely eliminated by adding an excess of the unlabeled NF-κB probe but not by the unlabeled AP1 probe (Fig. 5A, lanes 6 and 7). Anti-p50 antibody supershifted the complexes (Fig. 5A, lane 4) and anti-p65 antibody partially disrupted the DNA binding of the complexes (Fig. 5A, lane 5). To examine whether the Aβ-induced increase in nuclear NF-κB binding activity correlated with tyrosine kinase and PI3-kinase, Ra2 cells were preincubated with chemical inhibitors before treatment with Aβ. LY294002 reduced Aβ-induced binding to the NF-κB probe and piceatannol blocked the DNA-binding complex (Fig. 5B, lanes 4–7). These results indicate that Aβ enhances the binding of NF-κB to M-CSF promoter via the Syk tyrosine kinase and the PI3-kinase.

We have shown in the present study that Aβ proliferates microglia and induces M-CSF via the PI3-kinase/Akt/NFκB signal pathways. It has been reported that Aβ binds to CD36, which transduces signals via tyrosine kinase [6,20]. CD36 may participate in the initiation of intracellular signaling to M-CSF expression. RAGE also has been reported to induce NF-κB activation to M-CSF production [30]. Further works are needed to prove the receptors of Aβ, which induces PI3-kinase/Akt/NF-κB signal pathways to M-CSF mRNA expression. Aβ increases production of reactive oxygen species (ROS) and activates Akt in neural cells [23]. And in microglia CD36 mediates production of ROS in response to Aβ [31]. We found that antioxidants such as reduced glutathione and α-tocopherol slightly blocked M-CSF mRNA expression (data not shown). Also in microglia, ROS may partly participate in activating the signal cascade to M-CSF expression. It is important to reveal the relation among the receptors of Aβ, production of ROS and signal cascades.

Monsonego et al. [32] showed that activated microglia migrated outside the brain and could present Aβ peptide to T lymphocytes. Further analysis of microglial activation may reveal the immunological mechanism of AD, and may enhance the prospects of immune manipulation to prevent AD.

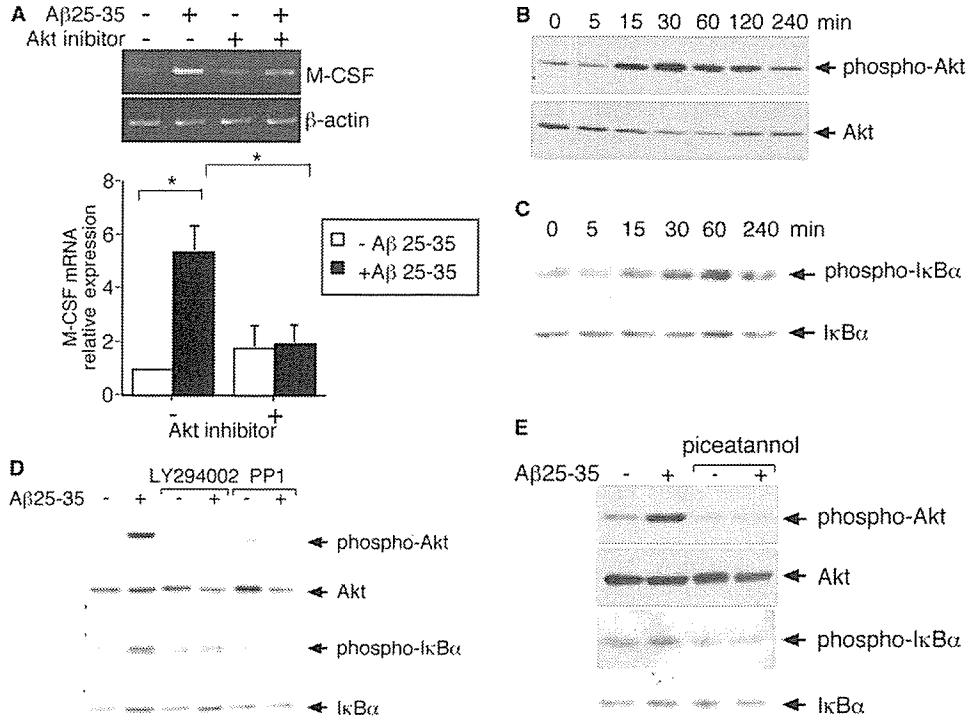

Fig. 4. Aβ-induced Akt and IκB phosphorylation through tyrosine kinase and PI3-kinase. (A) RT-PCR (top) and real-time PCR (bottom) of M-CSF mRNA. Ra2 cells were preincubated with or without 20 μM Akt inhibitor before treatment with 25 μM Aβ25–35 for 6 h. Data represent means ± S.D. values of three separate determinations. (*$P < 0.01$) (B–E) Immunoblotting analysis using anti-phospho Akt (Ser 473) or anti-phospho IκBα (Ser 32) antibody. The same blots were reprobed with anti-Akt or anti-IκB antibody. Ra2 cells were treated with Aβ25–35 for indicated times (B and C). Ra2 cells were preincubated with 25 μM LY294002 or 10 μM PP1 for 30 min or 50 μM piceatannol for 1 h before treatment with 50 μM Aβ25–35 for 30 min (D and E).

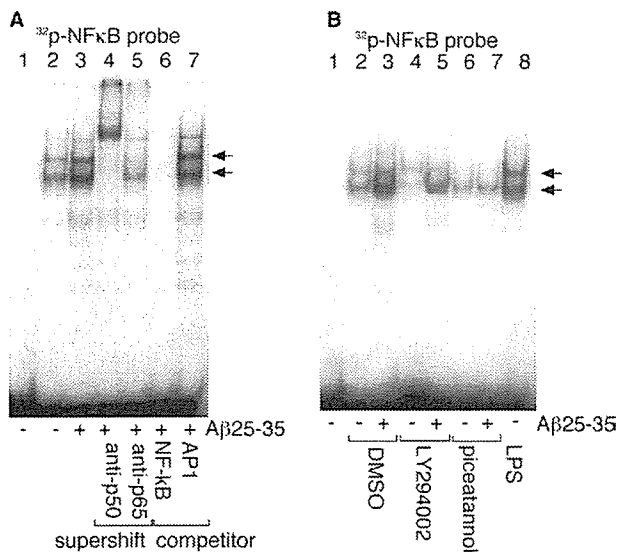

Fig. 5. NF-κB binding activity in EMSA. ^{32}P-labeled probe without nuclear extracts are showed in lane 1. (A) Ra2 cells were treated with 50 μM Aβ25–35 for 4 h (lanes 3–7). Anti-p50 or anti-p65 antibody was added to the extracts for supershift assay (lanes 4 and 5). Unlabeled competitor of NF-κB or AP1 probe was added to the extract (lanes 6 and 7). (B) Ra2 cells were preincubated with 25 μM LY294002 for 30 min (lanes 4 and 5) or 50 μM piceatannol for 1 h (lanes 6 and 7) before treatment with or without 50 μM Aβ25–35 for 4 h (lanes 2–7). Control cells were preincubated with DMSO (lanes 2 and 3). Nuclear extract of Ra2 cells treated with 1 μg/ml LPS for 4 h were used as a positive control (lane 8).

Acknowledgements: This study was supported by the Program for the Promotion of Fundamental Studies in Health Sciences of the Organization for Pharmaceutical Safety and Research (of Japan), and in part by grants-in-aid for Scientific Research from the Japanese Ministry of Education, Culture, Sports, Science and Technology.

References

[1] Akiyama, H., et al. (2000) Inflammation and Alzheimer's disease. Neurobiol. Aging 21, 383–421.
[2] Husemann, J., Loike, J.D., Anankov, R., Febbraio, M. and Silverstein, S.C. (2002) Scavenger receptors in neurobiology and neuropathology: their role on microglia and other cells of the nervous system. Glia 40, 195–205.
[3] El Khoury, J., Hickman, S.E., Thomas, C.A., Cao, L., Silverstein, S.C. and Loike, J.D. (1996) Scavenger receptor-mediated adhesion of microglia to beta-amyloid fibrils. Nature 382, 716–719.
[4] Paresce, D.M., Ghosh, R.N. and Maxfield, F.R. (1996) Microglial cells internalize aggregates of the Alzheimer's disease amyloid beta-protein via a scavenger receptor. Neuron 17, 553–565.
[5] El Khoury, J.B., Moore, K.J., Means, T.K., Leung, J., Terada, K., Toft, M., Freeman, M.W. and Luster, A.D. (2003) CD36 mediates the innate host response to beta-amyloid. J. Exp. Med. 197, 1657–1666, Epub 2003 Jun 1609.
[6] Bamberger, M.E., Harris, M.E., McDonald, D.R., Husemann, J. and Landreth, G.E. (2003) A cell surface receptor complex for fibrillar beta-amyloid mediates microglial activation. J. Neurosci. 23, 2665–2674.
[7] Huang, M.M., Bolen, J.B., Barnwell, J.W., Shattil, S.J. and Brugge, J.S. (1991) Membrane glycoprotein IV (CD36) is physically associated with the Fyn, Lyn, and Yes protein-tyrosine kinases in human platelets. Proc. Natl. Acad. Sci. USA 88, 7844–7848.

[8] Bull, H.A., Brickell, P.M. and Dowd, P.M. (1994) Src-related protein tyrosine kinases are physically associated with the surface antigen CD36 in human dermal microvascular endothelial cells. FEBS Lett. 351, 41–44.
[9] Jimenez, B., Volpert, O.V., Crawford, S.E., Febbraio, M., Silverstein, R.L. and Bouck, N. (2000) Signals leading to apoptosis-dependent inhibition of neovascularization by thrombospondin-1. Nat. Med. 6, 41–48.
[10] Verdier, Y. and Penke, B. (2004) Binding sites of amyloid beta-peptide in cell plasma membrane and implications for Alzheimer's disease. Curr. Protein Pept. Sci. 5, 19–31.
[11] Sawada, M., Imai, F., Suzuki, H., Hayakawa, M., Kanno, T. and Nagatsu, T. (1998) Brain-specific gene expression by immortalized microglial cell-mediated gene transfer in the mammalian brain. FEBS Lett. 433, 37–40.
[12] Sawada, M., Suzumura, A., Hosoya, H., Marunouchi, T. and Nagatsu, T. (1999) Interleukin-10 inhibits both production of cytokines and expression of cytokine receptors in microglia. J. Neurochem. 72, 1466–1471.
[13] Hattori, T., Takei, N., Mizuno, Y., Kato, K. and Kohsaka, S. (1995) Neurotrophic and neuroprotective effects of neuron-specific enolase on cultured neurons from embryonic rat brain. Neurosci. Res. 21, 191–198.
[14] Maehara, K., Hasegawa, T., Xiao, H., Takeuchi, A., Abe, R. and Isobe, K. (1999) Cooperative interaction of NF-kappaB and C/EBP binding sites is necessary for manganese superoxide dismutase gene transcription mediated by lipopolysaccharide and interferon-gamma. FEBS Lett. 449, 115–119.
[15] Terzi, E., Holzemann, G. and Seelig, J. (1994) Reversible random coil-beta-sheet transition of the Alzheimer beta-amyloid fragment (25–35). Biochemistry 33, 1345–1350.
[16] Shearman, M.S., Ragan, C.I. and Iversen, L.L. (1994) Inhibition of PC12 cell redox activity is a specific, early indicator of the mechanism of beta-amyloid-mediated cell death. Proc. Natl. Acad. Sci. USA 91, 1470–1474.
[17] Pike, C.J., Walencewicz-Wasserman, A.J., Kosmoski, J., Cribbs, D.H., Glabe, C.G. and Cotman, C.W. (1995) Structure-activity analyses of beta-amyloid peptides: contributions of the beta 25–35 region to aggregation and neurotoxicity. J. Neurochem. 64, 253–265.
[18] Araujo, D.M. and Cotman, C.W. (1992) Beta-amyloid stimulates glial cells in vitro to produce growth factors that accumulate in senile plaques in Alzheimer's disease. Brain Res. 569, 141–145.
[19] Nagele, R.G., Wegiel, J., Venkataraman, V., Imaki, H. and Wang, K.C. (2004) Contribution of glial cells to the development of amyloid plaques in Alzheimer's disease. Neurobiol. Aging 25, 663–674.
[20] Moore, K.J., El Khoury, J., Medeiros, L.A., Terada, K., Geula, C., Luster, A.D. and Freeman, M.W. (2002) A CD36-initiated signaling cascade mediates inflammatory effects of beta-amyloid. J. Biol. Chem. 277, 47373–47379.
[21] Combs, C.K., Johnson, D.E., Cannady, S.B., Lehman, T.M. and Landreth, G.E. (1999) Identification of microglial signal transduction pathways mediating a neurotoxic response to amyloidogenic fragments of beta-amyloid and prion proteins. J. Neurosci. 19, 928–939.
[22] Zhang, C., Qiu, H.E., Krafft, G.A. and Klein, W.L. (1996) A beta peptide enhances focal adhesion kinase/Fyn association in a rat CNS nerve cell line. Neurosci. Lett. 211, 187–190.
[23] Martin, D., Salinas, M., Lopez-Valdaliso, R., Serrano, E., Recuero, M. and Cuadrado, A. (2001) Effect of the Alzheimer amyloid fragment Abeta(25–35) on Akt/PKB kinase and survival of PC12 cells. J. Neurochem. 78, 1000–1008.
[24] Luo, Y., Sunderland, T. and Wolozin, B. (1996) Physiologic levels of beta-amyloid activate phosphatidylinositol 3-kinase with the involvement of tyrosine phosphorylation. J. Neurochem. 67, 978–987.
[25] Tang, Y., Yu, J. and Field, J. (1999) Signals from the Ras, Rac, and Rho GTPases converge on the Pak protein kinase in Rat-1 fibroblasts. Mol. Cell. Biol. 19, 1881–1891.
[26] Jiang, K., Zhong, B., Gilvary, D.L., Corliss, B.C., Hong-Geller, E., Wei, S. and Djeu, J.Y. (2000) Pivotal role of phosphoinositide-3 kinase in regulation of cytotoxicity in natural killer cells. Nat. Immunol. 1, 419–425.
[27] Romashkova, J.A. and Makarov, S.S. (1999) NF-kappaB is a target of AKT in anti-apoptotic PDGF signalling. Nature 401, 86–90.
[28] Traenckner, E.B., Pahl, H.L., Henkel, T., Schmidt, K.N., Wilk, S. and Baeuerle, P.A. (1995) Phosphorylation of human I kappa B-alpha on serines 32 and 36 controls I kappa B-alpha proteolysis and NF-kappa B activation in response to diverse stimuli. Embo J. 14, 2876–2883.
[29] Harrington, M.A., Edenberg, H.J., Saxman, S., Pedigo, L.M., Daub, R. and Broxmeyer, H.E. (1991) Cloning and characterization of the murine promoter for the colony-stimulating factor-1-encoding gene. Gene 102, 165–170.
[30] Lue, L.F., Walker, D.G., Brachova, L., Beach, T.G., Rogers, J., Schmidt, A.M., Stern, D.M. and Yan, S.D. (2001) Involvement of microglial receptor for advanced glycation endproducts (RAGE) in Alzheimer's disease: identification of a cellular activation mechanism. Exp. Neurol. 171, 29–45.
[31] Coraci, I.S., et al. (2002) CD36, a class B scavenger receptor, is expressed on microglia in Alzheimer's disease brains and can mediate production of reactive oxygen species in response to beta-amyloid fibrils. Am. J. Pathol. 160, 101–112.
[32] Monsonego, A., Imitola, J., Zota, V., Oida, T. and Weiner, H.L. (2003) Microglia-mediated nitric oxide cytotoxicity of T cells following amyloid beta-peptide presentation to Th1 cells. J. Immunol. 171, 2216–2224.

Available online at www.sciencedirect.com
ScienceDirect
Neuroscience Research 56 (2006) 294–299
Neuroscience Research
www.elsevier.com/locate/neures

Amyloid-β peptides induce several chemokine mRNA expressions in the primary microglia and Ra2 cell line via the PI3K/Akt and/or ERK pathway

Sachiko Ito [a], Makoto Sawada [b], Masataka Haneda [a], Yoshiyuki Ishida [c], Ken-ichi Isobe [a,*]

[a] *Department of Immunology, Nagoya University Graduate School of Medicine, 65 Turumai-cho, Showa-ku, Nagoya, Aichi 466-8520, Japan*
[b] *Department of Brain Life Science, Research Institute for Environmental Medicine, Nagoya University, Furo-cho, Chikusa-ku, Nagoya 464-8601, Japan*
[c] *Radioisotope Research Center, Nagoya University, Furo-cho, Chikusa-ku, Nagoya 464-8601, Japan*

Received 11 April 2006; accepted 26 July 2006
Available online 15 September 2006

Abstract

Alzheimer's disease (AD) is characterized by the presence of senile plaques composed primarily of amyloid-β peptide (Aβ) in the brain. Microglia have been reported to surround these Aβ plaques, which have opposite roles, provoking a microglia-mediated inflammatory response that contributes to neuronal cell loss or the removal of Aβ and damaged neurons. To perform these tasks microglia migrate to the sites of Aβ secretion. We herein analyzed the process of chemokine expression induced by Aβ stimulation in primary murine microglia and Ra2 microglial cell line. We found that Aβ1-42 induced the expressions of CCL7, CCL2, CCL3, CCL4 and CXCL2 in the microglia. The signal transduction pathway for the expression of CCL2 and CCL7 mRNA induced by Aβ1-42 was found to depend on phosphatidylinositol 3-kinase (PI3K)/Akt and extracellular signal-regulated kinase (ERK), whereas the pathway for CCL4 depended only on PI3K/Akt. These inflammatory chemokine expressions by Aβ stimulation emphasize the contribution of neuroinflammatory mechanisms to the pathogenesis of AD.

Keywords: Microglia; Alzheimer's disease; Amyloid β; Chemokine; Akt; ERK

1. Introduction

Alzheimer's disease (AD) is characterized by the presence of senile plaques composed primarily of amyloid-β peptide (Aβ) in the brain. Microglia have been reported to surround Aβ plaques (Haga et al., 1989; Itagaki et al., 1989). Aβ-induced microglia have been shown to produce reactive oxygen species, TNFα, IL1β, which have been demonstrated to cause the degeneration of nervous cells (Akiyama et al., 2000; Ishii et al., 2000; Blasko et al., 2004). On the other hand, microglia play an important role in the clearance of Aβ by phagocytosis, primarily through scavenger receptor class A (SR-A, CD204), scavenger receptor-BI (SR-BI) and CD36 (El Khoury et al., 1996; Paresce et al., 1996; Husemann et al., 2002). Other receptors such as receptor for advanced glycosylation end-products (RAGE), integrins and heparan sulfate proteoglycans, have also been reported to bind with Aβ (Verdier and Penke, 2004). CD36 binds to Aβ *in vitro* (Bamberger et al., 2003), and it is physically associated with members of the Src family tyrosine kinase (Huang et al., 1991; Bull et al., 1994), which transduce signals from this receptor (Jimenez et al., 2000).

Microglia as a macrophage-lineage cell may produce several chemokines, which induce microglial chemotaxis. It has recently been reported that microglia produce MCP-1 (CCL2) and other chemokines by Aβ stimulation through CD36 receptor (El Khoury et al., 2003). Another report examined the production of chemokines in THP-1 monocytes

Abbreviations: AD, Alzheimer's disease; Aβ, amyloid-β; ERK, extracellular signal-regulated kinase; FBS, fetal bovine serum; GM-CSF, granulocyte-macrophage colony stimulating factor; PBS, phosphate-buffered saline; PI3K, phosphatidylinositol 3-kinase

* Corresponding author. Tel.: +81 52 744 2135; fax: +81 52 744 2972.
E-mail address: kisobe@med.nagoya-u.ac.jp (K.-i. Isobe).

0168-0102/$ – see front matter
doi:10.1016/j.neures.2006.07.009

induced by Aβ (Giri et al., 2003). However, there have so far been no reports, which examined the whole series of inflammatory chemokine expression induced by Aβ in microglial cells. We herein extensively examined the whole series of inflammatory chemokine expression by Aβ stimulation using real-time PCR methods. By this examination we found that CCL2 (MCP-1), CCL3 (MIP-lα), CCL4 (MIP-1β), CCL7 (MCP-3) and CXCL2 were induced by Aβ1-42. Then we further analyzed the signaling pathway for CCL2, CCL4 and CCL7 mRNA expression induced by AB1-42 in the microglia.

2. Materials and methods

2.1. Materials

Synthetic human Aβ1-42 and Aβ1-40 were obtained from Peptide Institute Inc. (Osaka, Japan). Aβ1-42 and Aβ1-40 were dissolved in 0.1% NH_3 solution according to the manufacturer's instructions. Anti-phospho-Akt (Serine 473), anti-Akt, anti-phospho-ERKl/2 (Thr202/Tyr204) antibodies were from Cell Signaling (Beverly, MA). Anti-ERK antibody was from Santa Cruz (Santa Cruz, CA). Wortmannin and PD98059 were from Calbiochem (San Diego, CA). U0126 and SB203580 were from Promega (Madison, WI). All inhibitors were resolved in DMSO. Mouse recombinant granulocyte-macrophage colony-stimulating factor (mrGM-CSF) was from BD Pharmingen (San Diego, CA).

2.2. Cell culture

The microglial cell line Ra2 cells were established from neonatal C57BL/6J (H-2^b) mice using a non-enzymatic and non-virus-transformed procedure (Sawada et al., 1998). Ra2 cells proliferate in a culture medium containing GM-CSF. The medium for maintaining Ra2 cells was MGI medium [Eagle's MEM supplemented with 0.2% glucose, 5 μg/ml bovine Insulin (Sigma–Aldrich, St. Louis, MO), 10% fetal bovine serum (FBS, Invitrogen, Carlsbad, CA)] and 0.8 ng/ml mrGM-CSF (BD Pharmingen). Before Aβ-treatment, the Ra2 cells were cultured in an MGI medium without mrGM-CSF for 16 h. The primary microglia was prepared using newborn C57BL/6 mice as described previously (Sawada et al., 1999), and then they were cultured in MGI medium containing 0.8 ng/ml mrGM-CSF. The purity of primary microglial cultures was estimated to >95% based on the expression of CD11b marker using flow cytometry.

2.3. Quantitative real-time RT-PCR

Ra2 cells and primary microglial cells were plated in 6 cm diameter dishes at 1 × 10^6 cells/dish and treated with Aβ or 0.1% NH_3 solution as a control. Total RNA was isolated using an RNeasy mini kit (Qiagen, Hilden, Germany) according to the manufacturer's instructions. Two micrograms of total RNA was reverse transcribed to 20 μl cDNA using Superscript II Reverse Transcriptase (Invitrogen). Quantitative SYBR Green real-time PCR was performed on M×3000P (Promega) using the following program: 10 s at 95 °C, followed by 40 cycles of 5 s at 95 °C, 20 s at 60 °C. The reactions were carried out using 0.5 μl cDNA with SYBR Premix EX Taq (Takara, Shiga, Japan). The sequences of the primer for real-time PCR are depicted in Table 1. As an endogenous reference we used β-actin. Specificity of the PCR product was confirmed by examination of dissociation reaction plots. A distinct single peak indicated that single DNA sequence was amplified during PCR. In addition, end reaction products were visualized on ethdium bromide-stained 2.0% agarose gels. Appearance of a single band of the correct size confirmed specificity of the PCR. Quantitative analysis of gene expression was performed using the comparative cycle threshold (C_T) method, in which C_T is the threshold cycle number (Livak and Schmittgen, 2001). The target gene (target, i.e. CCL2) was normalized to an endogenous reference gene (β-actin). To indicate relative expression, we calculated using the expression $2^{-\Delta\Delta C_T}$, where $\Delta\Delta C_T = (C_{T,target} - C_{T,actin})_{treated\ sample} - (C_{T,target} - C_{T,actin})_{control\ sample}$. Each sample was tested in triplicate with quantitative PCR, and samples obtained from three independent experiments were used to calculate the means ± S.D.

Table 1
The sequences of the primer for real-time PCR

Target (pruduct size)	Sequence (5′–3′)
CCL2 (127 bp)	Sense: TGAATGTGAAGTTGACCCGT Antisense: AAGGCATCACAGTCCGAGTC
CCL3 (163 bp)	Sense: CCTCTGTCACCTGCTCAACA Antisense: GATGAATTGGCGTGGAATCT
CCL4 (237 bp)	Sense: CCCACTTCCTGCTGTTTCTC Antisense: GAGGAGGCCTCTCCTGAAGT
CCL5 (242 bp)	Sense: ATATGGCTCGGACACCACTC Antisense: GGGAAGCGTATACAGGGTCA
CCL6 (185 bp)	Sense: GCCACACAGATCCCATGTAA Antisense: GCAATGACCTTGTTCCCAGA
CCL7 (157 bp)	Sense: GCATGGAAGTCTGTGCTGAA Antisense: AGAAAGAACAGCGGTGAGGA
CCL8 (282 bp)	Sense: TCAGCCCAGAGAAGCTGACT Antisense: TCCAGCTTTGGCTGTCTCTT
CCL9 (244 bp)	Sense: CAAAGGAGGGCATTATGAGC Antisense: CCTTGCTGTGCCTTCAGACT
CCL12 (181 bp)	Sense: GTCCTCAGGTATTGGCTGGA Antisense: GGGTCAGCACAGATCTCCTT
CCL19 (236 bp)	Sense: CAAGAACAAAGGCAACAGCA Antisense: CGGCTTTATTGGAAGCTCTG
CCL20 (154 bp)	Sense: CGTCTGCTCTTCCTTGCTTT Antisense: CTTCATCGGCCATCTGTCTT
CXCL2 (258 bp)	Sense: TCCAGAGCTTGAGTGTGACG Antisense: AGGCACATCAGGTACGATCC
β-Actin (298 bp)	Sense: AGTGTGACGTTGACATCCGT Antisense: GCAGCTCAGTAACAGTCCGC

2.4. Immunoblotting

The cells (1 × 10^6 cells/dish) were lysed in sample buffer (62.5 mM Tris–HCl, pH 6.8, 2% SDS, 10% glycerol, 5% 2-mercaptoethanol, and 5% bromophenol blue). Protein concentrations were quantified by the Bradford assay using the Bio-Rad protein assay (Bio-Rad, Herucules, CA). Then total protein (50 μg per lane) was resolved by SDS-PAGE and then was transferred to PVDF membranes (Millipore, Billerica, CA). The blots were incubated with anti-phospho ERK or anti-phospho Akt overnight at 4 °C and then treated with HRP-conjugated secondary antibody. Signals were detected by ECL system (Amersham Biosciences, Little Chalfont, UK). The blots were stripped by incubation in stripping buffer (100 mM 2-mercaptoethanol, 2% SDS, 62.5 mM Tris–HCl, pH 6.8) and reprobed with anti-ERK or anti-Akt.

2.5. Statistical analysis

The results are expressed as the means ± S.D. Comparisons among means were performed using ANOVA, followed by the Scheffe's test. The two-tailed Student's *t*-test was used for comparisons between two means.

3. Results

3.1. Production of several chemokines by Aβ-induced microglia

We analyzed the effect of Aβ on the expression of chemokines, in the microglia, which has been shown to be secreted by inflammatory macrophages. The microglial cell

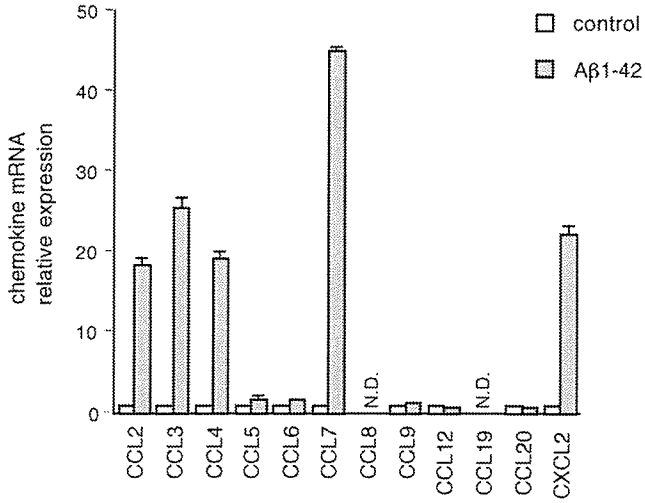

Fig. 1. Aβ1-42 induced the expression of chemokine. Ra2 cells were treated with 10 μM Aβ1-42 or 0.1% NH_3 solution as a control for 16 h. Real-time PCR of a series of chemokine and β-actin mRNA were performed. The chemokine mRNA expression was normalized to β-actin. The results indicated relative expression of chemokine in Aβ-treated cells compared with control cells. The data represent the means ± S.D. of triplicate of three separate experiments. N.D.: the PCR signal was not detected.

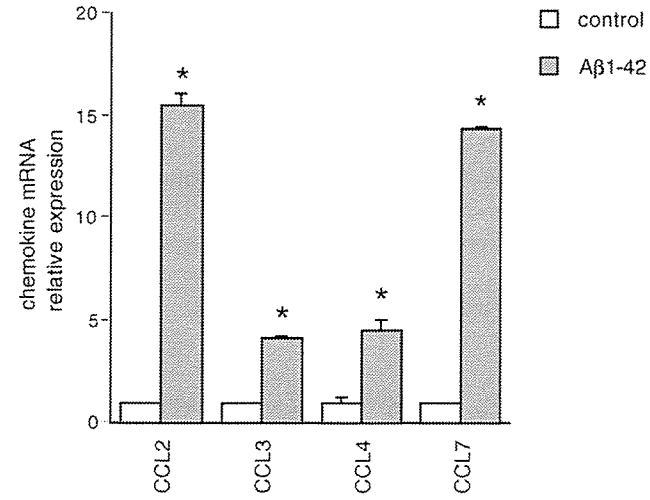

Fig. 2. Induction of the chemokine mRNA expression by Aβ1-42 in primary microglia. Primary cultured microglial cells were treated with 10 μM Aβ1-42 or 0.1% NH_3 solution as a control for 16 h. Extracted mRNA was quantified by real-time PCR. The results indicated relative expression of CCL2, CCL3, CCL4 and CCL7 in Aβ-treated cells compared with control cells. The data represent the means ± S.D. of triplicate of three separate experiments. $^{*}p < 0.001$ vs. each control of chemokine.

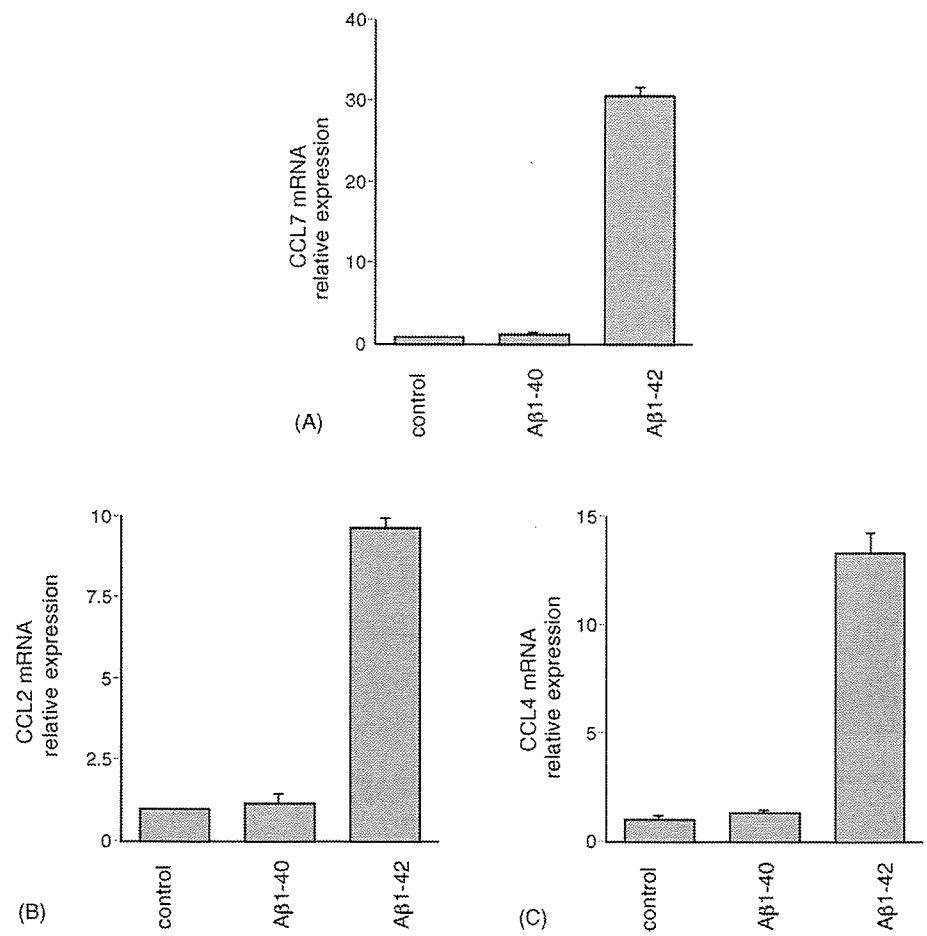

Fig. 3. The mRNA expression of chemokine induced with Aβ1-42 or Aβ1-40. Ra2 cells were stimulated 10 μM Aβ1-42 and 10 μM Aβ1-40 for 16 h. Extracted mRNA was quantified by real-time PCR. The results indicated relative expression of CCL7 (A), CCL2 (B), CCL4 (C) in Aβ-treated cells compared with control cells. The data represent the means ± S.D. of triplicate of three separate experiments.

line Ra2 was treated with 10 μM Aβ1-42 for 16 h, and the expression of chemokines was examined by quantitative real-time PCR. We found the expression of CCL7 mRNA to be highly increased by Aβ1-42 stimulation (Fig. 1). The expressions of CCL2, CCL3, CCL4 and CXCL2 were also increased by Aβ1-42. In the primary microglial cells cultured from C57BL/6 mouse newborn brain, CCL2, CCL3, CCL4 and CCL7 mRNA expression were induced by Aβ1-42 (Fig. 2).

3.2. Aβ1-42 but not Aβ1-40 induces chemokine production in the microglia

As shown in Fig. 3A, Aβ1-42 but not Aβ1-40 induces CCL7 mRNA. In our assay, the high induction of CCL7 mRNA expression was examined, when Aβ1-42 was added to the culture. Interestingly, Aβ1-40 was not found to induce CCL7 (Fig. 3A). The expression of CCL2 and CCL4 also were induced by Aβ1-42 but not Aβ1-40 (Fig. 3B and C).

3.3. Aβ induces CCL2 and CCL7 mRNA via the Erk and PI3-kinase signal cascade

Next, we examined the signal cascades for Aβ-induced CCL7 mRNA expression by using several chemical inhibitors (Fig. 4A). Wortmannin, a phosphatidylinositol 3-kinase (PI3K) inhibitor, clearly inhibited the CCL7 mRNA expression induced by Aβ. Both U0126 and PD98059, MEK inhibitors, also inhibited the increase in CCL7 mRNA expression.

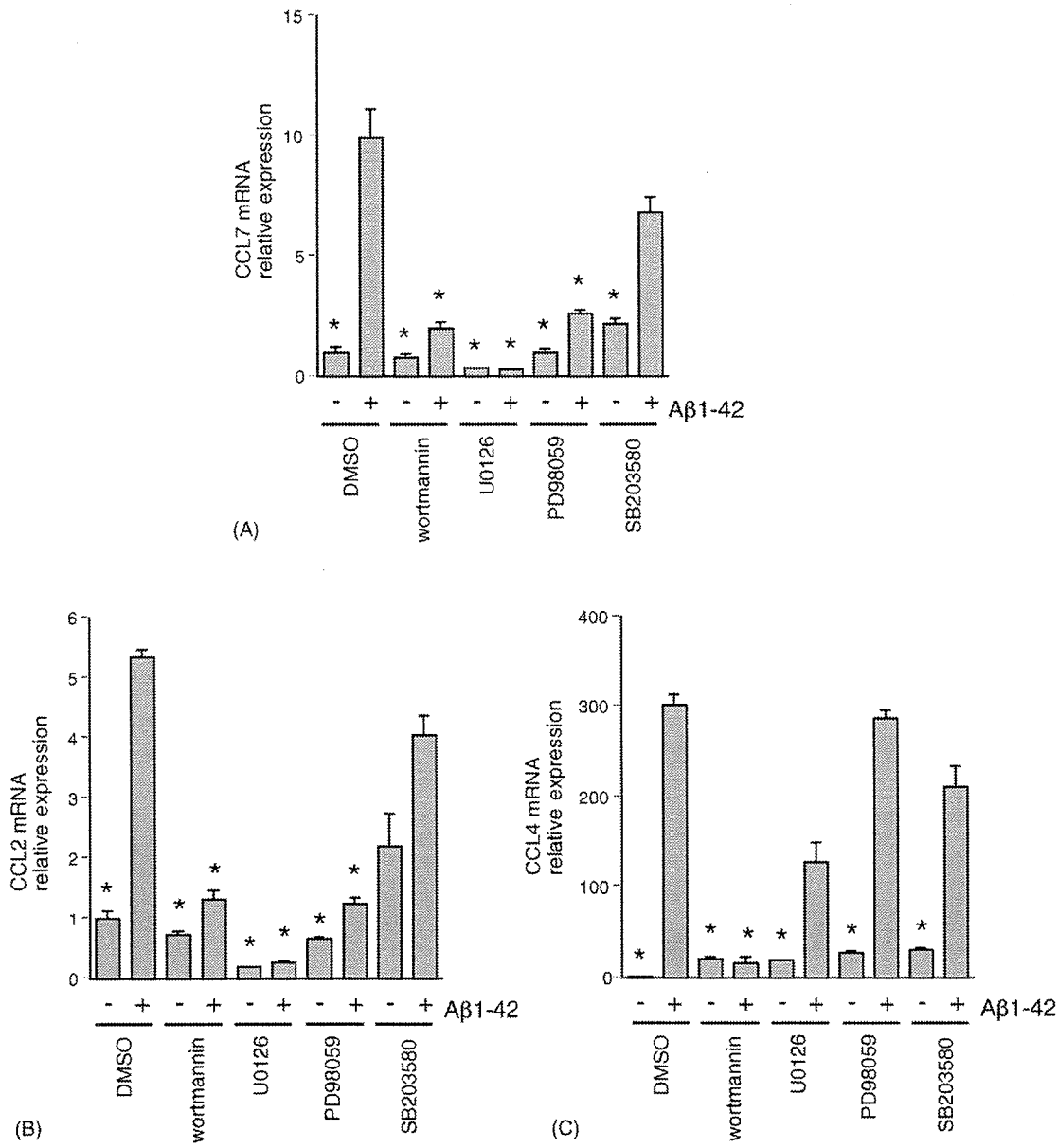

Fig. 4. Signal transduction for chemokine mRNA expression induced by Aβ1-42. Ra2 cells were preincubated with 200 nM wortmannin, 10 μM U0126, 10 μM PD98059 or 10 μM SB203580 for 30 min before the addition of 10 μM Aβ1-42 or 0.1% NH_3 solution as a control for 6 h. Extracted mRNA was quantified by real-time PCR. The results indicated relative expression of CCL7 (A), CCL2 (B) and CCL4 (C) in Aβ-treated cells compared with control cells. The data represent the means ± S.D. of triplicate of three separate experiments. $^{*}p < 0.001$ vs. Aβ-treated cells (DMSO).

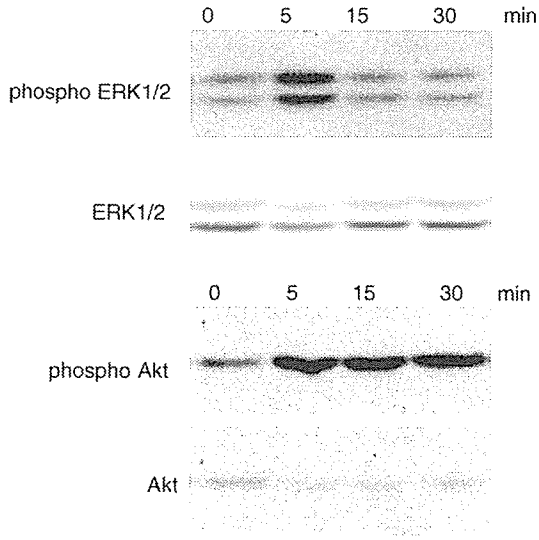

Fig. 5. Aβ1-42 induces the phosphorylation of ERK and Akt. Ra2 cells were treated with 10 μM Aβ1-42 for indicated times. Cell lysates were analyzed by immunoblotting using anti-phospho ERKI/2 or anti-phospho Akt antibody. The same blots were reprobed with anti-ERK or anti-Akt antibody.

However, SB203580, a p38 inhibitor, did not inhibit the CCL7 mRNA expression. These results indicate that Aβ induces increase in CCL7 mRNA via both the PI3K/Akt and ERK signaling pathways. For comparison, we also examined the signaling pathway of CCL2 and CCL4. The signaling pathway for the CCL2 mRNA was similar to that for CCL7, namely both the PI3K/Akt inhibitor and the MEK inhibitors blocked the increase in CCL2 mRNA expression (Fig. 4B). However, the CCL4 expression was clearly blocked by the PI3K/Akt inhibitor but not blocked by the MEK inhibitors (Fig. 4C). Immunoblotting analysis revealed that the phosphorylation of the ERK was induced by Aβ1-42 at a peak of 5 min (Fig. 5). In addition, we confirmed that Akt was phosphorylated at serine 473 by Aβ1-42.

4. Discussion

Tissue resident macrophage is activated by various stimuli such as infection, and secretes a range of cytokines and chemokines. Chemokines recruit leukocytes (macrophage and granulocyte) to sites of the tissue injury. In the case of AD, initial injurious stimulus is Aβ. Microglia as one of the macrophage-lineage cells might produce inflammatory chemokine induced by Aβ. The data presented in this paper demonstrate that the CCL2, CCL3, CCL4, CCL7 and CXCL2 mRNA expressions are induced by Aβ1-42 in microglia. Among these chemokines, the induction of CCL7 mRNA expression was the highest. MCP-1 (CCL2) and MIP-1β (CCL4) have been shown to be expressed in THP-1 monocyte stimulated by Aβ (Giri et al., 2003). However, it has not been reported that the induction of CCL7 mRNA by Aβ stimulation. In our results, Aβ1-42 but not Aβ1-40 induced the expression of CCLs. Because Aβ1-42 is easy to aggregate but Aβ1-40 tends to remain monomer, the difference of the induction of CCL mRNA expression may depend on the aggregation status of these peptides.

We have herein shown that the Aβ-induced CCL7 and CCL2 mRNA expressions correlated with the activation of the ERK and PI3K/Akt signaling cascades in the microglia. Several groups have examined that Aβ activated ERK pathway in microglia and THP-1 monocytes (McDonald et al., 1998; Combs et al., 1999). Giri et al. showed that Aβ induced the activation of MCP-1 (CCL2) via ERK pathway in THP-1 cells (Giri et al., 2003). Their results partially correlate with ours. We further showed that the PI3K/Akt pathway is also involved in CCL2 expression induced by Aβ. In our result, the induction of CCL7 and CCL2 mRNA need ERK and PI3K/Akt, but that of CCL4 correlated with only PI3K. A common transcriptional mechanism may therefore participate in CCL7 and CCL2 mRNA expression.

Although the function of chemokine in AD pathogenesis has not been clarified, the chemokine expression in AD patients has recently been studied. A Dutch-Italian Alzheimer Research group demonstrated the expressions of interferon-γ-inducible protein-10 (IP-10), CCL2, IL8 in CSF and serum of AD to be up-regulated in comparison to the control (Galimberti et al., 2003). A Swedish group reported an increase of CCL2 in the CSF and serum of AD patients (Sun et al., 2003). These studies suggest the importance of chemokine in AD pathogenesis. Our *in vitro* work will give some suggestions to the clinical studies of AD pathogenesis.

In conclusion, we have demonstrated that Aβ induces several chemokines (CCL2, CCL3, CCL4, CCL7 and CXCL2) in microglia. This study to our knowledge is the first to fully demonstrate the expression pattern of macrophage-lineage chemokine in microglia induced by Aβ. These chemokines may have important function in the AD pathogenesis. The signaling pathways from Aβ to chemokine mRNA expression should help us to develop therapeutic methods of AD.

Acknowledgements

This study was supported by the Program for the Promotion of Fundamental Studies in Health Sciences of the Organization for Pharmaceutical Safety and Research (of Japan), and in part by grants-in-aid for Scientific Research from the Japanese Ministry of Education, Culture, Sports, Science and Technology.

References

Akiyama, H., Barger, S., Barnum, S., Bradt, B., Bauer, J., Cole, G.M., Cooper, N.R., Eikelenboom, P., Emmerling, M., Fiebich, B.L., Finch, C.E., Frautschy, S., Griffin, W.S., Hampel, H., Hull, M., Landreth, G., Lue, L., Mrak, R., Mackenzie, I.R., McGeer, P.L., O'Banion, M.K., Pachter, J., Pasinetti, G., Plata-Salaman, C., Rogers, J., Rydel, R., Shen, Y., Streit, W., Strohmeyer, R., Tooyoma, I., Van Muiswinkel, F.L., Veerhuis, R., Walker, D., Webster, S., Wegrzyniak, B., Wenk, G., Wyss-Coray, T., 2000. Inflammation and Alzheimer's disease. Neurobiol. Aging 21, 383–421.

Bamberger, M.E., Harris, M.E., McDonald, D.R., Husemann, J., Landreth, G.E., 2003. A cell surface receptor complex for fibrillar beta-amyloid mediates microglial activation. J. Neurosci. 23, 2665–2674.

Blasko, I., Stampfer-Kountchev, M., Robatscher, P., Veerhuis, R., Eikelenboom, P., Grubeck-Loebenstein, B., 2004. How chronic inflammation can affect the brain and support the development of Alzheimer's disease in old age: the role of microglia and astrocytes. Aging Cell 3, 169–176.

Bull, H.A., Brickell, P.M., Dowd, P.M., 1994. Src-related protein tyrosine kinases are physically associated with the surface antigen CD36 in human dermal microvascular endothelial cells. FEBS Lett. 351, 41–44.

Combs, C.K., Johnson, D.E., Cannady, S.B., Lehman, T.M., Landreth, G.E., 1999. Identification of microglial signal transduction pathways mediating a neurotoxic response to amyloidogenic fragments of beta-amyloid and prion proteins. J. Neurosci. 19, 928–939.

El Khoury, J.B., Moore, K.J., Means, T.K., Leung, J., Terada, K., Toft, M., Freeman, M.W., Luster, A.D., 2003. CD36 mediates the innate host response to beta-amyloid. J. Exp. Med. 197, 1657–1666.

El Khoury, J., Hickman, S.E., Thomas, C.A., Cao, L., Silverstein, S.C., Loike, J.D., 1996. Scavenger receptor-mediated adhesion of microglia to beta-amyloid fibrils. Nature 382, 716–719.

Galimberti, D., Schoonenboom, N., Scarpini, E., Scheltens, P., 2003. Chemokines in serum and cerebrospinal fluid of Alzheimer's disease patients. Ann. Neurol. 53, 547–548.

Giri, R.K., Selvaraj, S.K., Kalra, V.K., 2003. Amyloid peptide-induced cytokine and chemokine expression in THP-1 monocytes is blocked by small inhibitory RNA duplexes for early growth response-1 messenger RNA. J. Immunol. 170, 5281–5294.

Haga, S., Akai, K., Ishii, T., 1989. Demonstration of microglial cells in and around senile (neuritic) plaques in the Alzheimer brain. An immunohistochemical study using a novel monoclonal antibody. Acta Neuropathol. (Berlin) 77, 569–575.

Huang, M.M., Bolen, J.B., Barnwell, J.W., Shattil, S.J., Brugge, J.S., 1991. Membrane glycoprotein IV (CD36) is physically associated with the Fyn, Lyn, and Yes protein-tyrosine kinases in human platelets. Proc. Natl. Acad. Sci. U.S.A 88, 7844–7848.

Husemann, J., Loike, J.D., Anankov, R., Febbraio, M., Silverstein, S.C., 2002. Scavenger receptors in neurobiology and neuropathology: their role on microglia and other cells of the nervous system. Glia 40, 195–205.

Ishii, K., Muelhauser, F., Liebl, U., Picard, M., Kuhl, S., Penke, B., Bayer, T., Wiessler, M., Hennerici, M., Beyreuther, K., Hartmann, T., Fassbender, K., 2000. Subacute NO generation induced by Alzheimer's beta-amyloid in the living brain: reversal by inhibition of the inducible NO synthase. FASEB J. 14, 1485–1489.

Itagaki, S., McGeer, P.L., Akiyama, H., Zhu, S., Selkoe, D., 1989. Relationship of microglia and astrocytes to amyloid deposits of Alzheimer disease. J. Neuroimmunol. 24, 173–182.

Jimenez, B., Volpert, O.V., Crawford, S.E., Febbraio, M., Silverstein, R.L., Bouck, N., 2000. Signals leading to apoptosis-dependent inhibition of neovascularization by thrombospondin-1. Nat. Med. 6, 41–48.

Livak, K.J., Schmittgen, T.D., 2001. Analysis of relative gene expression data using real-time quantitative PCR and the $2^{-\Delta\Delta C_T}$ method. Methods 25, 402–408.

McDonald, D.R., Bamberger, M.E., Combs, C.K., Landreth, G.E., 1998. beta-Amyloid fibrils activate parallel mitogen-activated protein kinase pathways in microglia and THP1 monocytes. J. Neurosci. 18, 4451–4460.

Paresce, D.M., Ghosh, R.N., Maxfield, F.R., 1996. Microglial cells internalize aggregates of the Alzheimer's disease amyloid beta-protein via a scavenger receptor. Neuron 17, 553–565.

Sawada, M., Imai, F., Suzuki, H., Hayakawa, M., Kanno, T., Nagatsu, T., 1998. Brain-specific gene expression by immortalized microglial cell-mediated gene transfer in the mammalian brain. FEBS Lett. 433, 37–40.

Sawada, M., Suzumura, A., Hosoya, H., Marunouchi, T., Nagatsu, T., 1999. Interleukin-10 inhibits both production of cytokines and expression of cytokine receptors in microglia. J. Neurochem. 72, 1466–1471.

Sun, Y.X., Minthon, L., Wallmark, A., Warkentin, S., Blennow, K., Janciauskiene, S., 2003. Inflammatory markers in matched plasma and cerebrospinal fluid from patients with Alzheimer's disease. Dement Geriatr. Cogn. Disord. 16, 136–144.

Verdier, Y., Penke, B., 2004. Binding sites of amyloid beta-peptide in cell plasma membrane and implications for Alzheimer's disease. Curr. Protein Pept. Sci. 5, 19–31.

nature medicine

17-AAG, an Hsp90 inhibitor, ameliorates polyglutamine-mediated motor neuron degeneration

Masahiro Waza[1,2], Hiroaki Adachi[1,2], Masahisa Katsuno[1], Makoto Minamiyama[1], Chen Sang[1], Fumiaki Tanaka[1], Akira Inukai[1], Manabu Doyu[1] & Gen Sobue[1]

Heat-shock protein 90 (Hsp90) functions as part of a multichaperone complex that folds, activates and assembles its client proteins. Androgen receptor (AR), a pathogenic gene product in spinal and bulbar muscular atrophy (SBMA), is one of the Hsp90 client proteins. We examined the therapeutic effects of 17-allylamino-17-demethoxygeldanamycin (17-AAG), a potent Hsp90 inhibitor, and its ability to degrade polyglutamine-expanded mutant AR. Administration of 17-AAG markedly ameliorated motor impairments in the SBMA transgenic mouse model without detectable toxicity, by reducing amounts of monomeric and aggregated mutant AR. The mutant AR showed a higher affinity for Hsp90-p23 and preferentially formed an Hsp90 chaperone complex as compared to wild-type AR; mutant AR was preferentially degraded in the presence of 17-AAG in both cells and transgenic mice as compared to wild-type AR. 17-AAG also mildly induced Hsp70 and Hsp40. 17-AAG would thus provide a new therapeutic approach to SBMA and probably to other related neurodegenerative diseases.

Hsp90, which accounts for 1–2% of cytosolic protein, is one of the most abundant cellular chaperone proteins[1]. It functions in a multicomponent complex of chaperone proteins including Hsp70, Hop (Hsp70 and Hsp90 organizing protein), Cdc37, Hsp40 and p23. Hsp90 is involved in the folding, activation and assembly of several proteins, known as Hsp90 client proteins[1]. As numerous oncoproteins have been shown to be Hsp90 client proteins[1], Hsp90 inhibitors have become a new strategy in antitumor therapy[2]. Geldanamycin, a classical Hsp90 inhibitor, is known as a potent antitumor agent[2]; however, it has not been used in clinical trials because of its liver toxicity[3]. 17-AAG is a new derivative of geldanamycin that shares its important biological activities[4] but shows less toxicity[5].

Hsp90 requires several interacting, co-chaperone proteins to exert its function on Hsp90 client proteins in Hsp90 complexes[1], of which two main forms exist[6]. One complex is a proteasome-targeting form associated with Hsp70 and Hop, and the other is a stabilizing form with Cdc37 and p23 (refs. 7,8). Particularly, p23 is thought to modulate Hsp90 activity in the last stages of the chaperoning pathway, leading to stabilized Hsp90 client proteins[9]. Hsp90 inhibitors, including 17-AAG, inhibit the progression of the Hsp90 complex toward the stabilizing form[10–12], and shift it to the proteasome-targeting form[7,8], resulting in enhanced proteasomal degradation of the Hsp90 client protein[7,13–18].

Because 17-AAG has less toxicity and higher selectivity for client oncoproteins[19], 17-AAG is now in clinical trials for a wide range of malignancies[20]. Additionally, Hsp90 inhibitors also function as Hsp inducers[20,21]. Several previous studies have suggested that Hsp90 inhibitors could be applied to nononcological diseases as neuroprotective agents based on their induction of Hsps[22–28].

Androgen receptor (AR) is one of the Hsp90 client proteins[15], and is a pathogenic gene product of spinal and bulbar muscular atrophy (SBMA), one of the polyglutamine (polyQ) diseases[29]. This disease is characterized by premature muscular exhaustion, slow progressive muscular weakness, atrophy and fasciculation in bulbar and limb muscles[30]. PolyQ diseases are inherited neurodegenerative disorders caused by the expansion of a trinucleotide CAG repeat in the causative genes[31]. In SBMA, the number of polymorphic CAG repeats is normally 14–32, whereas it is expanded to 40–62 CAGs in the *AR* gene[32]. A correlation exists between CAG repeat size and disease severity[33]. The pathologic features of SBMA are motor neuron loss in the spinal cord and brainstem[30], and diffuse nuclear accumulation and nuclear inclusions of the mutant AR in the residual motor neurons and certain visceral organs[34].

We have already examined several therapeutic approaches in a mouse model of SBMA[35–38]. As a consequence, we confirmed that castration and leuprorelin, a luteinizing hormone–releasing hormone agonist that reduces testosterone release from the testis, substantially rescued motor dysfunction and nuclear accumulation of mutant AR in male transgenic mice[35,37]. Although this hormonal therapy was effective, it poses the unavoidable difficulty of severe sexual dysfunction[37]. In addition, this therapy cannot be applied to other polyQ diseases.

Here, we present a new and potent strategy for SBMA therapy with 17-AAG, an Hsp90 inhibitor. Given that Hsp90 inhibitors have two major activities, preferential client protein degradation and Hsp induction, we hypothesized that 17-AAG would degrade mutant AR more effectively than wild-type AR.

[1]Department of Neurology, Nagoya University Graduate School of Medicine, 65 Tsurumai-cho, Showa-ku, Nagoya 466-8550, Japan. [2]These authors contributed equally to this work. Correspondence should be addressed to G.S. (sobueg@med.nagoya-u.ac.jp).

Received 25 February; accepted 10 August; published online 11 September 2005; doi:10.1038/nm1298

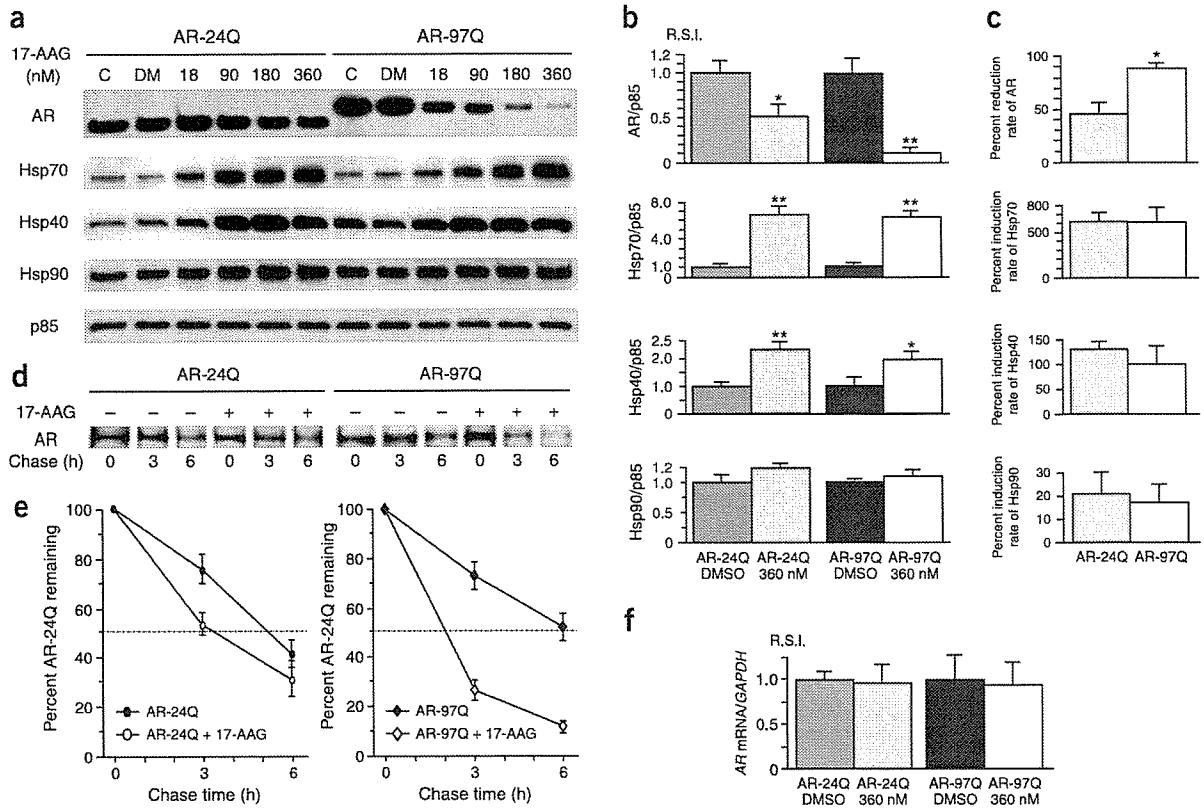

Figure 1 Effect of 17-AAG on the AR or chaperones in cultured-cell models. (**a**,**b**) Although the immunoblot and densitometric analysis showed a dose-dependent decline in both wild-type (AR-24Q) and mutant (AR-97Q) AR expression in response to 17-AAG, the mutant AR decreased more than did the wild-type. 17-AAG markedly increased the expression of Hsp70 and Hsp40, especially for Hsp70, but only slightly increased Hsp90 expression. (**c**) The decrease in mutant AR after treatment with 17-AAG was much higher than that of wild-type AR (88.9% versus 45.9%, $P = 0.0063$). Values are expressed as mean ± s.e.m. ($n = 5$). (**d**) Pulse-chase analysis of two forms of AR. Data from one representative experiment for wild-type and mutant AR. (**e**) Pulse-chase assessment of the half-life of wild-type and mutant AR. The amounts of AR-24Q and AR-97Q remaining in the absence and presence of 17-AAG are indicated. Values are expressed as mean ± s.e.m. ($n = 4$). (**f**) Real-time RT-PCR of wild-type and mutant *AR* mRNA. Quantities are shown as the ratio to *GAPDH* mRNA. The wild-type and mutant *AR* mRNA levels were similar under 17-AAG treatments. Values are expressed as mean ± s.e.m. ($n = 4$). $^*P < 0.025$, $^*P < 0.005$.

In this study, we examine the effects of 17-AAG on a cultured-cell model and the transgenic mouse model of SBMA. We show that the mutant AR exists more frequently as a stabilized Hsp90 chaperone complex than does the wild-type AR, and that 17-AAG selectively degrades the mutant AR. Administration of 17-AAG inhibits neuronal nuclear accumulation of the mutant AR and considerably ameliorates motor phenotypes of the SBMA model mouse.

RESULTS

Effect of 17-AAG on expression of AR and Hsps *in vitro*

To address the question of whether 17-AAG promotes the degradation of polyQ-expanded AR, we treated SH-SY5Y cells highly expressing the wild-type (AR-24Q) or mutant (AR-97Q) AR for 48 h with the indicated doses of 17-AAG or with DMSO as control. Although immunoblot analysis showed a dose-dependent decline in both wild-type and mutant AR expression after treatment with 17-AAG (**Fig. 1a**), the monomeric mutant AR decreased significantly more than did the wild-type ($P = 0.0063$; **Fig. 1b,c**), suggesting that the mutant AR is more sensitive to 17-AAG than is the wild-type. The expression of Hsp70 and Hsp40 were also markedly increased after treatment with 17-AAG, but Hsp90 was only slightly increased (**Fig. 1a,b**). There were no significant differences, however, in the levels of Hsp70, Hsp40 and Hsp90 induction between the wild-type and mutant AR (**Fig. 1c**).

To determine whether the decrease in AR resulted from protein degradation or from changes in RNA expression, we assessed the turnover of wild-type and mutant AR with a pulse-chase labeling assay. Without treatment, the wild-type and mutant AR were degraded in a similar manner, as previously reported[39,40]. In the presence of 17-AAG, however, the wild-type and mutant AR had half-lives of 3.5 h and 2 h, respectively (**Fig. 1d,e**), whereas levels of mRNA encoding the wild-type and mutant AR were quite similar (**Fig. 1f**). Cell viability did not differ between wild-type and mutant AR transfected cells (data not shown). These data indicate that 17-AAG preferentially degrades the mutant AR protein without cellular toxicity or alteration of mRNA levels.

To address why 17-AAG preferentially degrades mutant AR, we determined the levels of Hsp90, Hop and p23 associated with wild-type or mutant AR in SH-SY5Y cells without 17-AAG treatment (**Fig. 2a**). Hop and p23 are two essential components of multi-chaperone Hsp90 complexes[1]. Without 17-AAG treatment, coimmunoprecipitation from the cell lysates with antibodies to AR showed that p23 was more highly associated with mutant than with wild-type AR (**Fig. 2a,b**). The total levels of Hsp90, Hop and p23 were similar in the cells transfected with either wild-type or mutant AR (**Fig. 2a**).

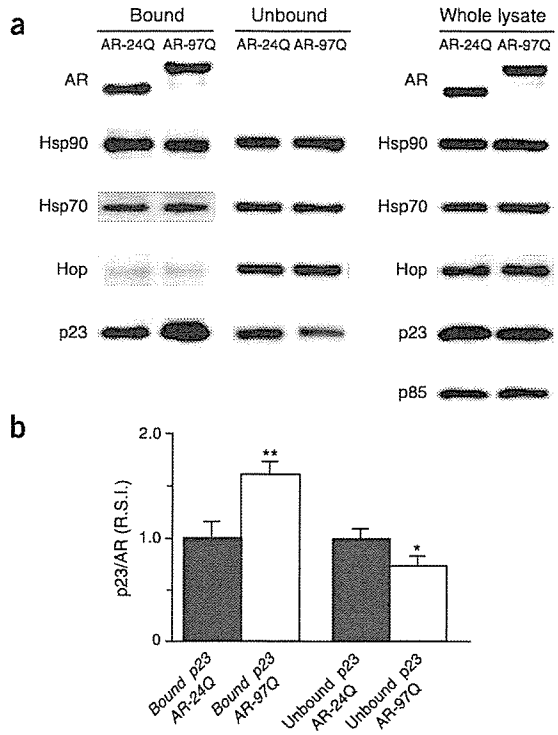

Figure 2 Immunoprecipitation of wild-type and mutant AR in cultured-cell models. (**a**) Wild-type and mutant AR were immunoprecipitated from cell lysates with an AR-specific antibody and immunoblotted with antibodies to the indicated western blot proteins. There was more mutant AR present in multichaperone complexes with p23 than there was wild-type AR. There were no differences in total expression levels of AR, Hsp90, Hsp70, Hop and p23 between wild-type and mutant AR–expressing cells. Control immunoprecipitations without antibodies did not immunoprecipitate any co-chaperones (data not shown). (**b**) The densitometric analysis of p23 in the bound and unbound fractions shows there was 1.6 times as much p23 associated with mutant AR than there was with the wild-type ($P < 0.01$). This experiment was repeated with five sets of cells with equivalent results. Values are expressed as mean ± s.e.m. ($n = 5$). $^*P < 0.05$, $^{**}P < 0.01$. R.S.I., relative signal intensity.

We next examined the status of the Hsp90 chaperone complex in wild-type and mutant AR-expressing cultured cells treated with 17-AAG. Immunoprecipitation with AR-specific antibody showed that Hsp90 chaperone complex–associated Hop was markedly increased, and p23 decreased depending on the dose of 17-AAG (**Fig. 3a,b**), suggesting that treatment with 17-AAG resulted in the shifting of the AR-Hsp90 chaperone complex from a mature stabilizing form with p23 to a proteasome-targeting form with Hop. The loss of p23 from the mutant AR-Hsp90 complex was significantly higher ($P < 0.005$) than that from the wild-type AR-Hsp90 complex (**Fig. 3c**). The degradation of wild-type and mutant AR by 17-AAG was completely blocked by the proteasome inhibitor MG132 (**Fig. 3d**), suggesting that the pharmacological degradation by 17-AAG was dependent on the proteasome system, as previously reported[17,18]. Furthermore, these results strongly suggest that mutant AR is more likely to be in the Hsp90-p23 multichaperone complexes, which eventually enhances 17-AAG–dependent proteasomal degradation of mutant AR.

Moreover, mutant AR was markedly decreased after treatment with 17-AAG even when induction of Hsp70 and Hsp40 was blocked by the protein-synthesis inhibitor cycloheximide (**Supplementary Fig. 1** online), suggesting that 17-AAG contributes to the preferential degradation of mutant AR mainly through Hsp90 chaperone complex formation and subsequent proteasome-dependent degradation rather than through induction of Hsp70 and Hsp40.

17-AAG ameliorates phenotypic expression of SBMA mice

We administered 17-AAG (2.5 or 25 mg/kg) to male transgenic mice carrying full-length human AR-24Q or AR-97Q. The disease progression of AR-97Q mice treated with 25 mg/kg 17-AAG (Tg-25) was

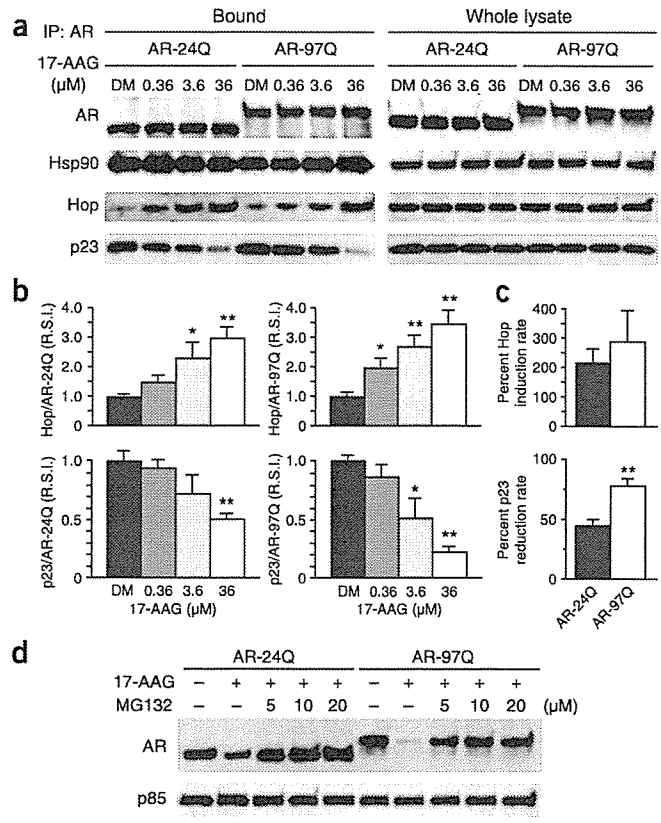

Figure 3 Pharmacological change in the AR-Hsp90 complex, and the correlation to proteasomal degradation. (**a**) Immunoblots of lysates of transfected cells treated with 17-AAG. Lysates were immunoprecipitated with AR-specific antibody. The short time exposure to 17-AAG did not decrease the amount of mutant AR. There were dose-dependent changes in both Hop and p23 after treatment with 17-AAG; however, no dissociation of Hsp90 from the mutant AR complex was seen. There were no changes in the expression of Hop, p23 and Hsp90 in whole lysates in the presence of 17-AAG. (**b**) Densitometric analysis of Hop and p23 in the bound fractions. There was a marked increase in the amount of Hop, and a marked decrease in p23 in both wild-type and mutant AR-bound Hsp90 complexes after treatment with 17-AAG. R.S.I., relative signal intensity. (**c**) Comparisons of induction rate of Hop and reduction rate of p23 in the Hsp90 complexes of wild-type and mutant AR. Although there was no significant difference in the induction rate of Hop between the wild-type and mutant AR complexes, the reduction rate of p23 was significantly higher in the mutant AR complex compared with that in the wild-type complex (43.8% versus 79.0%, $P < 0.005$). Values are expressed as means ± s.e.m. ($n = 5$). (**d**) Effect of 17-AAG on AR expression under the inhibition of proteasomal degradation. The mutant AR was more markedly reduced than wild-type AR after 17-AAG treatments; however, this pharmacological degradation was completely blocked by MG132 in both cases. DM, DMSO. $^*P < 0.025$, $^*P < 0.005$.

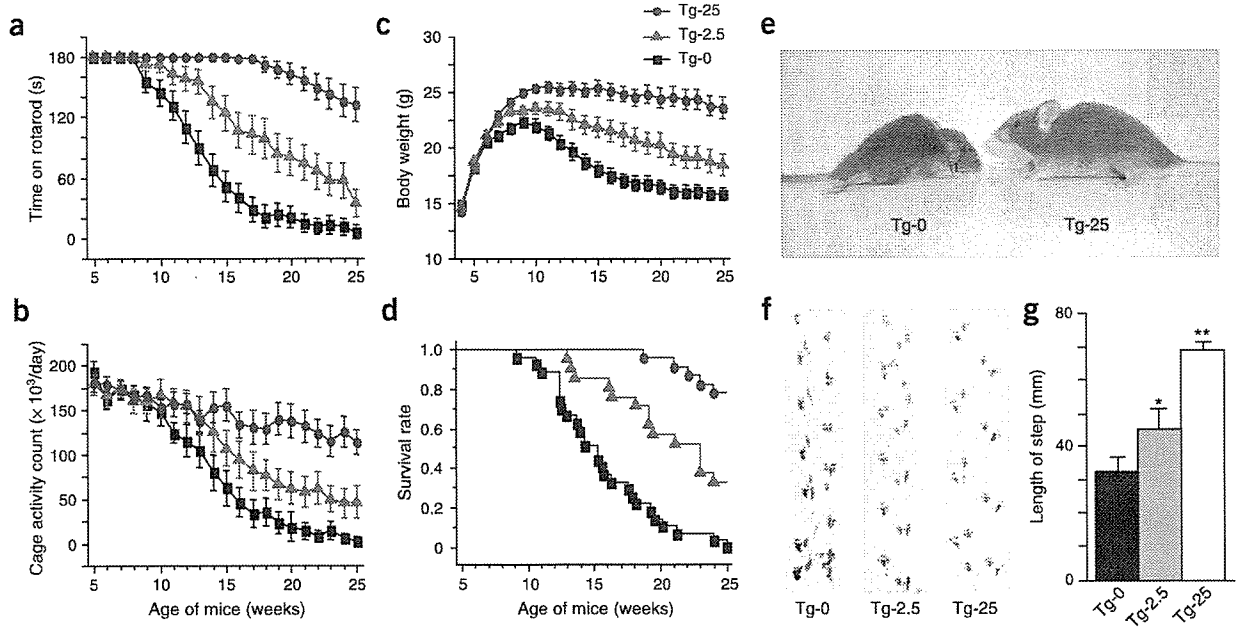

Figure 4 Effects of 17-AAG on behavioral and visible phenotypes in male AR-97Q mice. (**a**) Rotarod task ($n = 27$), (**b**) cage activity ($n = 18$), (**c**) body weight ($n = 27$) and (**d**) survival rate ($n = 27$) of Tg-0, Tg-2.5 and Tg-25 mice. All parameters were significantly different between the Tg-0 and Tg-25 ($P < 0.005$ for all parameters). A Kaplan-Meier plot shows the prolonged survival of Tg-2.5 and Tg-25 compared with Tg-0, which had all died by 25 weeks of age ($P = 0.004$, $P < 0.001$, respectively). (**e**) Representative photographs of a 16-week-old Tg-0 (left) shows an obvious difference in size, and illustrates muscular atrophy and kyphosis compared with an age-matched Tg-25 (right). (**f**) Footprints of representative 16-week-old Tg-0, Tg-2.5 and Tg-25 mice. Front paws are indicated in red and hind paws in blue. (**g**) The length of steps was measured in 16-week-old Tg-0, Tg-2.5 and Tg-25 mice. Each column shows an average of steps of the hind paw. Values are expressed as means ± s.e.m. ($n = 6$). *$P < 0.025$, **$P < 0.005$.

markedly ameliorated, and that of mice treated with the 2.5 mg/kg 17-AAG (Tg-2.5) was mildly ameliorated (**Fig. 4a–d**). The untreated transgenic male mice (Tg-0) showed motor impairment assessed by the rotarod task as early as 9 weeks after birth, whereas Tg-25 mice showed initial impairment only 18 weeks after birth and with less deterioration than Tg-0 mice (**Fig. 4a**). Tg-2.5 mice showed intermediate levels of impairment in rotarod performance (**Fig. 4a**). The locomotor cage activity of Tg-0 mice was also markedly decreased at 10 weeks compared with the other two groups, which showed decreases in activity at 13 (Tg-2.5) and 16 (Tg-25) weeks of age (**Fig. 4b**). Tg-0 mice lost weight significantly earlier and more profoundly than the Tg-2.5 ($P < 0.025$) and Tg-25 mice ($P < 0.005$; **Fig. 4c**). Treatment with 17-AAG also significantly prolonged the survival rate of Tg-2.5 ($P = 0.004$) and Tg-25 mice ($P < 0.001$) as compared to Tg-0 mice (**Fig. 4d**). 17-AAG was less effective at the close of 2.5 mg/kg than 25 mg/kg in all parameters tested. The lines were not distinguishable in terms of body weight at birth; however, by 16 weeks, Tg-0 mice showed obvious differences in body size, muscular atrophy and kyphosis compared to Tg-25 mice (**Fig. 4e**). Additionally, Tg-0 mice showed motor weakness, with short steps and dragging of the legs, whereas Tg-25 mice showed almost normal ambulation (**Fig. 4f,g**).

When we immunohistochemically examined mouse tissues for mutant AR using the 1C2 antibody, which specifically recognizes expanded polyQ, we observed a marked reduction in 1C2-positve nuclear accumulation in the spinal motor neurons (**Fig. 5a**) and muscles (**Fig. 5b**) of Tg-25 mice compared with those of Tg-0 mice. Glial fibrillary acidic protein (GFAP)-specific antibody staining showed an apparent reduction of reactive astrogliosis in Tg-25 compared with Tg-0 mice in the spinal anterior horn (**Fig. 5c**). Muscle histology also showed marked amelioration of neurogenic muscle atrophy in the AR-97Q mice treated with 17-AAG (**Fig. 5d**). We confirmed a significant reduction of 1C2-positive nuclear accumulation in both spinal cord ($P < 0.01$) and skeletal muscle ($P < 0.05$) by quantitative assessment (**Fig. 5e**). AR-24Q mice and normal littermates treated with 17-AAG showed no altered phenotypes (data not shown).

To evaluate the toxic effects of 17-AAG, we examined blood samples from 25-week-old mice treated with 25 mg/kg 17-AAG for 20 weeks. Measurements of aspartate aminotransferase, alanine aminotransferase, blood urea nitrogen and serum creatinine showed that treatment with 17-AAG resulted in neither infertility nor liver or renal dysfunction in the AR-97Q male mice at the dose of 25 mg/kg (**Supplementary Fig. 2** online).

Mutant AR is preferentially degraded by 17-AAG *in vivo*

As the mutant AR was preferentially degraded as compared to the wild-type AR in the presence of 17-AAG *in vitro*, we also examined the level of AR in the SBMA mouse model. Western blot analysis of lysates of the spinal cord and muscle of AR-97Q mice showed high molecular–weight mutant AR protein complex retained in the stacking gel as well as a band of monomeric mutant AR, whereas only the band of wild-type monomeric AR was visible in tissues from the AR-24Q mice (**Fig. 6a,b**). Treatment with 17-AAG notably diminished both the high molecular–weight complex and the monomer of mutant AR in the spinal cord and muscle of the AR-97Q mice, but only slightly diminished the wild-type monomeric AR in AR-24Q mice (**Fig. 6a,b**). Treatment with 17-AAG decreased the amount of the monomeric AR in AR-97Q mice by 64.4% in the spinal cord and 45.0% in the skeletal muscle, whereas these amounts were only 25.9% and 12.5%, respectively, in AR-24Q mice (**Fig. 6a,b**). Thus, the reduction rate of the monomeric mutant AR was significantly higher than the wild-type

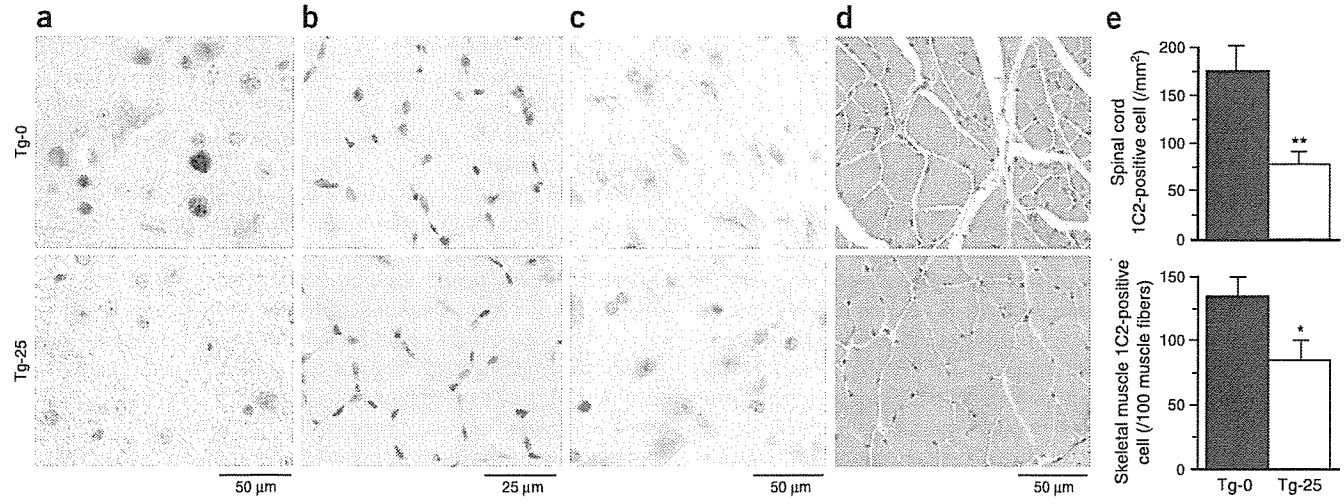

Figure 5 Effects of 17-AAG on the histopathology of male AR-97Q mice. (**a**,**b**) Immunohistochemical staining with 1C2-specific antibody showed marked differences in diffuse nuclear staining and nuclear inclusions between Tg-0 and Tg-25 mice in the spinal anterior horn and skeletal muscle, respectively. (**c**) Immunohistochemical staining with GFAP-specific antibody also showed an obvious reduction of reactive astrogliosis in the spinal anterior horn of mice treated with 17-AAG. (**d**) Hematoxylin and eosin staining of the muscle in Tg-0 mice showed obvious grouped atrophy and small angulated fibers, which were not seen in Tg-25 mice. (**e**) There was a significant reduction in 1C2-positive cell staining in the spinal cord ($P < 0.01$) and skeletal muscle ($P < 0.05$) in Tg-25 as compared to Tg-0 mice. Values are expressed as mean ± s.e.m. ($n = 6$). $^*P < 0.05$, $^{**}P < 0.01$.

AR in both spinal cord ($P < 0.001$) and skeletal muscle ($P < 0.01$; **Fig. 6c**). The levels of wild-type and mutant *AR* mRNA were similar in the respective mice treated with 17-AAG (**Fig. 6d**). We also performed filter-trap assays for quantitative analyses of both the large molecular aggregated and soluble forms of the mutant AR[36]. Both forms of trapped AR-97Q protein were markedly reduced in the spinal cord and muscle of Tg-25 mice, whereas those from the AR-24Q were not (**Supplementary Fig. 3** online). These observations strongly indicate that 17-AAG markedly reduces not only the monomeric mutant AR protein but also the high molecular–weight mutant AR complex, because of the preferential degradation of the mutant AR.

Western blot analysis showed that the levels of Hsp70 and Hsp40 in spinal cord were increased by 47.1% and 29.5%, respectively, and in muscle by 29.2% and 24.7%, respectively (**Supplementary Fig. 4** online) after treatment with 17-AAG. These pharmacological effects of chaperone induction were statistically significant ($P < 0.05$ for all parameters), but not as marked as the 17-AAG–induced mutant AR reduction, and were also not as pronounced as those arising from genetic manipulation in our previous study[36].

Hsp90 inhibitors nonspecifically activate heat shock responses through a dissociation of the heat-shock transcription factor (HSF-1) from the Hsp90 complex[27,41]. Although the expression of

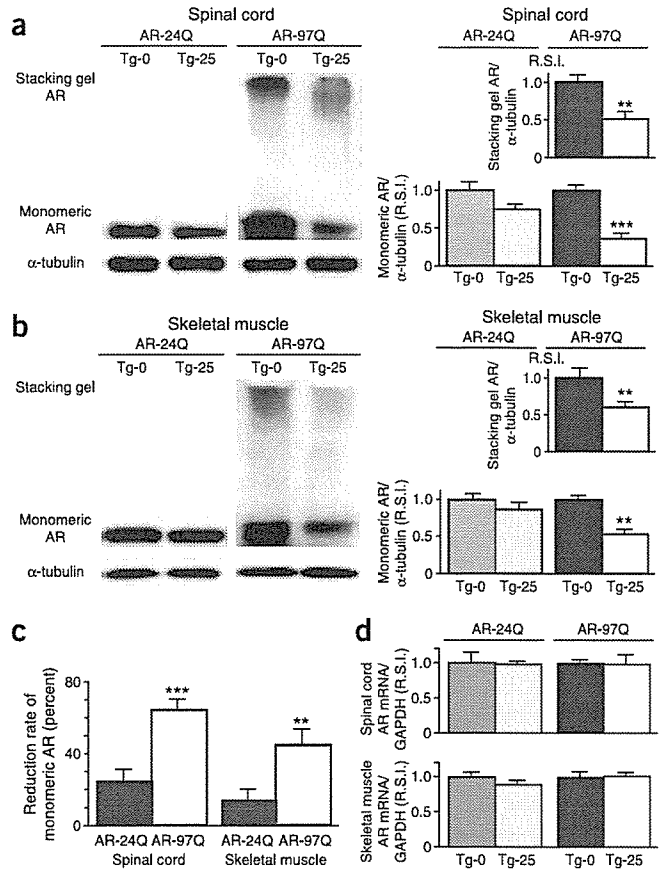

Figure 6 Effects of 17-AAG on AR expression in male AR-24Q or 97Q mice. (**a**,**b**) Western blot analysis of the spinal cord and muscle of AR-24Q and AR-97Q mice probed with AR-specific antibody. In both spinal cord and muscle of mice treated with 17-AAG, there was a significant decrease in the amount of mutant AR in the stacking gel and monomeric mutant AR in AR-97Q mice, but only slightly less monomeric wild-type AR in AR-24Q mice compared with that from untreated control mice. (**c**) Comparison of reduction rate of wild-type and mutant AR. Densitometric analysis showed that the 17-AAG–induced reduction of monomeric mutant AR was significantly greater than that of the wild-type monomeric AR. 17-AAG resulted in a 64.4% decline in monomeric mutant AR in the spinal cord, and a 45.0% decline in the skeletal muscle, whereas there was only a 25.9% decline in the spinal cord and a 12.5% decline in the skeletal muscle of AR-24Q mice. These results show significant differences of the reduction rate between wild-type and mutant AR in both spinal cord and skeletal muscle. Values are expressed as mean ± s.e.m. ($n = 5$). $^*P < 0.05$, $^{**}P < 0.01$, $^{***}P < 0.001$. (**d**) Real-time RT-PCR of wild-type and mutant *AR* mRNA *in vivo*. The expression levels of wild-type and mutant *AR* mRNA in transgenic mouse spinal cord and skeletal muscle were similar under 17-AAG treatments. Values are expressed as mean ± s.e.m. ($n = 3$).